České vysoké učení technické v Praze
Fakulta jaderná a fyzikálně inženýrská

Katedra fyziky
Obor: Fyzikální inženýrství
Zaměření: Fyzika a technika termojaderné fúze

Optimalizace provozu a zpracování dat diagnostiky tokamakového plazmatu pomocí Thomsonova rozptylu

Optimization of operation and data processing of tokamak plasma diagnostic based on Thomson scattering

RESEARCH STUDY

Author: Miroslav Šos
Supervisor: Ing. Petr Böhm, Ph.D.
Year: 2015

Před svázáním místo téhle stránky $\boxed{\text{vložíte zadání práce}}$ s podpisem děkana (bude to jediný oboustranný list ve Vaší práci) !!!!

Název práce:

Optimalizace provozu a zpracování dat diagnostiky tokamakového plazmatu pomocí Thomsonova rozptylu

Author: Miroslav Šos

Obor: Fyzikální inženýrství

Druh práce: Bakalářská práce

Vedoucí práce: Ing. Petr Böhm, Ph.D.
Ústav fyziky plazmatu, Akademie věd České Republiky, v.v.i.

Abstrakt: Abstract in Czech

Klíčová slova: Termojaderná fúze, tokamak COMPASS, diagnostika Thomsonova rozptylu, atd...

Title:

Optimization of operation and data processing of tokamak plasma diagnostic based on Thomson scattering

Author: Miroslav Šos

Abstract: Abstract in English

Key words: Thermonuclear fusion, COMPASS tokamak, Thomson scattering diagnostics, etc...

Contents

Introduction

Reliable diagnostic system is the principal aspect of each experimental research devices, including tokamaks. Tokamaks are being build and operated for the last 60 years, as they are one of several concepts that are able to confine and experiment with plasma in order to achieve sustainable thermonuclear fusion as a future source of energy. Plasma in tokamaks reaches extraordinary parameters, for example concerning its temperature, which could rise up to hundred millions of degrees Celsius. Therefore, requirements are extremely high on technology, materials, diagnostics and basically all included systems.

Diagnostics based on Thomson scattering (TS) is one of the few, that can provide measurements of electron temperature and density profiles, while does not affect plasma significantly. However, demands on the diagnostics performance and precision are very high in many aspects.

The first chapter of this study is dedicated to the theory of Thomson scattering and relevant plasma physics to understand TS diagnostics and the issues that are related to its operation and construction properly. To illustrate the implementation of such diagnostic system, TS on the COMPASS tokamak is described in the second chapter. Major effort is devoted to the description of crucial components with emphasis on those discussed afterwards in the text.

TS diagnostics becomes feasible only if high-powered laser are used. Alignment of the laser beam plays a key role in order to achieve high-quality measurements. The first section of the experimental part of this study is dedicated to the process of laser alignment by means of observation of the laser beam position by a camera and optimising subsequent correction with automated motorised mirrors.

In addition, precise spectral and absolute calibrations together with accurate data acquisition and processing are indispensable in order to provide reliable plasma diagnostic. Therefore second part is dedicated to systems that are included in the data processing system. Since the installation of TS on the COMPASS tokamak, commercial programming language IDL was used as a tool for calculation. New set of routines based on the open source programming language Python is one of the results of this study. The system is currently being finished and tested. Mitigation of stray light impact and optimization of the routines for fitting the detected scattered signal are the main issues that were proposed in the new method.

Chapter 1

Theoretical part

Following chapter concerns theoretical basics of plasma physics and processes which are relevant to the related topic of plasma scattering of electromagnetic radiation, namely Rayleigh, Raman and Thomson scattering. Elemental statements defining plasma nature and behaviour will be given and detailed features and processes based on previous assumptions will be described. Plasma conditions inside experimental devices are stated in order to understand key aspects that have to be considered to perform reliable measurement and diagnostics.

Having described basic plasma physics, theory of Thomson scattering itself is covered in following section. Principles of mentioned phenomenon are supplemented by equations signifying total scattered power and radiated spectrum for the purpose of predicting the character of scattered radiation. Presented results ensure the possibility for this type of diagnostic due to the fact that the character of scattered light reflects plasma parameters, specifically temperature and density.

1.1 Basic plasma physics

As the temperature of a material raises, its state changes from solid to liquid, then from liquid to gas. If the temperature increases even higher, certain amount of atoms become ionised. Though, plasma cannot be referred to as any ionised gas, because certain degree of ionisation show each gaseous medium. Even the air surrounding us is partly ionised by cosmic radiation. Therefore plasma is defined as a *quasi-neutral medium with free charge carriers that behaves collectively*.

1.1.1 Plasma behaviour

Quasi-neutrality is a characteristic feature of a certain volume, which on a microscopic scale shows in average the same quantity of positive and negative charges, is neutral when observed as a whole from the outside. As stated before, plasma consists of free charge carriers and consequently is conductive and reacts on external magnetic and electric field. As a result it is possible to shape and confine plasma by magnetic field. On the other hand it might bring undesirable effects, e.g. drifts, waves and instabilities.

The third mentioned property was collective behaviour of plasma. Moving charged particles generate electromagnetic field that alter the motion of other charged particles present in plasma. Thermal motion of particles may cause local perturbation in density or potential, thus creating electric field that can affect plasma on relatively long distances compared to those between two particles. As a result, plasma is a system of charged particles that generate fields to which the plasma reacts in turn.

The term quasi-neutrality is closely related to Debye shielding, fundamental phenomenon of plasma which is responsible for the neutrality on a macroscopic scale. Shielding mechanism can be described on a situation when a free test charge is placed to the plasma environment. Charged particles interact strongly by means of Coulomb force[1] that is proportional to $1/r$, where r represents the relative distance of particles. Charges with opposite signs are drawn towards each other and those with the same sign are driven away. Shielding is applied regardless of the sign of charge of the test particle, thus let us assume a positive charge carrier.

Negatively charged particles are attracted to the test charge whereas positive are repulsed, thus causing the plasma polarization. Generated electrostatic force exponentially decreases the potential of the test charge. Characteristic distance λ_D of described phenomenon is called Debye shielding length, which has a major role in plasma physics.

Plasma frequency is a result of the collective behaviour. A brief derivation is given below. Let us consider the case where small perturbations occurs in otherwise uniform plasma. Ions are approximately three orders of magnitude heavier than electrons thus are assumed stationary in relation to the electron motion. Due to the emerged displacement of electrons, electric charges appear inducing an electric field. Induced field accelerates electrons in the direction inward to the perturbation in order to suppress the disequilibrium. As a result of the electron inertia oscillation appears with the characteristic frequency ω_p. It is called electron plasma frequency and is defined as 1.1, where n_0, e and m_e represents initial electron density, electron charge and mass, respectively, and ε_0 is vacuum permittivity [13, p.8].

$$\omega_p^2 = \frac{n_0 e^2}{\varepsilon_0 m_e} \tag{1.1}$$

Electron plasma waves has this exact frequency and are the basic demonstrations of the collective behaviour of plasma. Plasma is a medium that requires much more complex and sophisti-

[1]Coulomb force is a long-range force, on short distances particles interact by means of *nuclear forces*, which are neglected in this case.

cated approach in order to describe other features, including other types of waves, drifts, plasma stability and instability, or transport mechanisms. Their description is out of the extent of this work but could be found in [13, 25], [9, czech only].

Unique behaviour and extraordinary phenomena are making plasma highly attractive object of physical and engineering research for more than one hundred years since its discovery in 1879 by Crookes.

1.1.2 Plasma conditions in tokamaks

Majority of current fusion[2] research projects is aimed at the thermonuclear approach, when the sufficient amount of energy-emerging reactions is achieved using high temperatures.

In general, the fundamental endeavour of thermonuclear fusion research is to achieve high values of plasma parameters, temperature and density, and its containment in that ideally stable situation as long as possible. Plasma parameters sufficient for thermonuclear fusion process are given by Lawson criterion 1.2, which states the fundamental condition for achieving sustainable thermonuclear source of energy. Quantities n,T and τ_E represent plasma density, temperature and the confinement time of stored energy defined in the same equation as a ratio of plasma energy W_p and power of loses P_L, respectively. The expression following the equal sing refers to the most convenient yet not the ideal fusion reaction between deuterium **D** and tritium **T**.

$$n\tau_E \geq f(T) = \frac{60k_BT}{\varepsilon_f < \sigma v >} \qquad\qquad \tau_E = \frac{W_p}{P_L} \tag{1.2}$$

On the basis of Lawson criterion he already in 1955 stated:

"Even with the most optimistic possible assumptions it is evident that the conditions for the operation of a useful thermonuclear reactor are very severe". [10]

Two principal and several approaches between them struggling with these severe requirements had emerged, namely inertial (ICF) and magnetic confinement fusion (MCF) are the two opposite ways. For the purposes of this work only the MCF is briefly described. Tokamak device, as a leading concept in thermonuclear fusion research in general, is based on magnetic confinement of plasma. Using high currents in several types of magnetic coils strong external magnetic field is created in a shape of a torus, therefore a vessel for plasma confinement is toroidal. Folding together with magnetic field produced by electric current flowing through the plasma, once is created within the tokamak vessel, results in theoretically stable helical field structure.

[2]*fusion* - in the sense of nuclear fusion, a reaction in which two or more atomic nuclei come close enough to form one or more different atomic nuclei and subatomic particles. [wikipedia]

Once a discharge is initiated, plasma becomes controlled, shaped, heated and otherwise affected in order to reach specific experimental goals. Typical range of values of key parameters during standard tokamak COMPASS operation is summarised in Tab. 1.1.

Parameter ╲ Device	**COMPASS**	**ASDEX-U**	**JET**	**ITER**
B_T [T]	0.9 - 2.1	3.9	3.5	11.8
I_p [MA]	0.4	2.0	3.2 - 4.6	15.0
t_d [s]	1	10	20	60 - 3600
n_e [10^{20} m^{-3}]	0.8	2.0	1.5	1.1
T_e [keV]	2	10	10	15
ω_p^2 [10^{23} s^{-2}]	2.545	6.364	4.773	3.500

Tab. 1.1: Table of approximate values of various parameter when operated in a standard mode, where B_T, I_p and t_d refers to amplitude of toroidal magnetic field, plasma current at maximum and discharge length and n_e and T_e represents plasma density and temperature, respectively. [6, 7, 12, 14]

Electron temperature is given in energy units (eV), typical units for plasma physics which correspond to the energy of the thermal motion. The last row in the table represents plasma frequency mentioned above, which has a reference to the way electromagnetic waves is transferred by plasma. The quantity is shown for future purposes.

1.2 General theory of Thomson scattering

Thomson scattering, firstly described by Nobel prize laureate J. J. Thomson, is the scattering of electromagnetic radiation by a free charged particle. More precisely the process is defined as the acceleration of a free charged particle by the incident field of an electromagnetic wave and the subsequent re-radiation by the electron of electromagnetic radiation into other directions [20, p. 2]. Process is schematically pictured in Fig. 1.1. Incident wave approaches free charge particle which is accelerated by it and starts to radiate creating pictured scattered wave in isotropic manner.

Diagnostic system based on Thomson scattering is a very powerful and non-perturbing technique used in plasma physics research and it provides detailed information about electron (ion) temperature and density. As stated below Thomson scattering cross-section is very low, thus high-intensity monochromatic light sources (Q-switched lasers [citation]) are indispensable in order to achieve sufficient production of scattered radiation. Electromagnetic waves produced by laser travel through plasma respecting disperse relation derived for instance in [13].

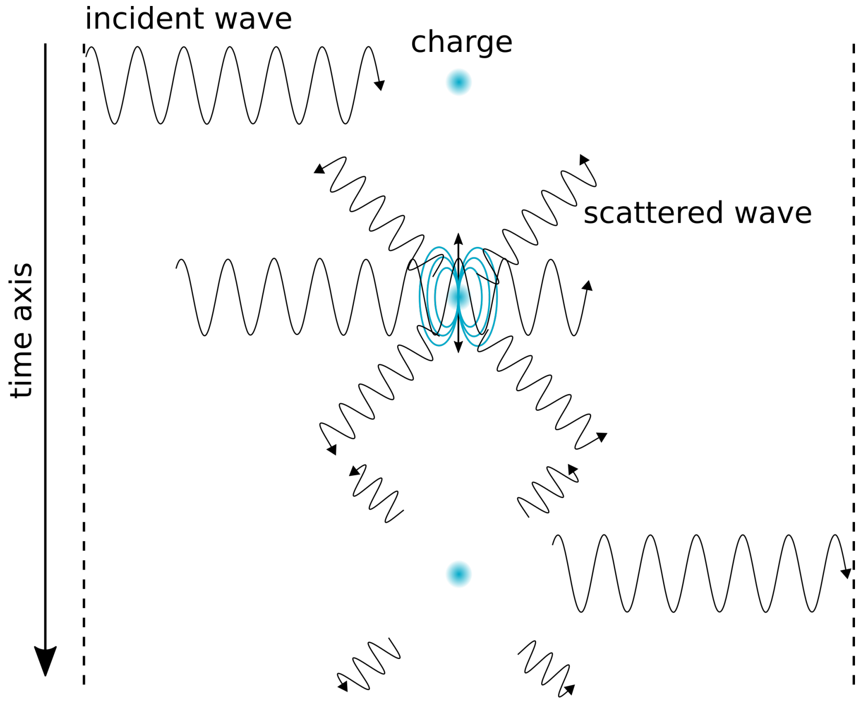

Fig. 1.1: Scheme of the process of scattering by a free charge particle, inspiration [8, p. 8].

1.2.1 Thomson scattering process

Following subsection will describe the process of Thomson scattering. As mentioned before it is based on wave-particle interaction. From this point on, only electron induced Thomson scattering will be discussed. Similar derivations might be done for the one induced by ions, but as stated below ion scattering is orders of magnitude less significant. Incident electromagnetic (EM) wave accelerates a free charged particle, electron, which experience the radiation at a different frequency due to Doppler effect, as a result of the electron's relative motion to the EM source with non-zero velocity. Accelerated electrons emit radiation, which is also Doppler shifted, due to the relative motion of the electron to the observer. Therefore scattered spectrum is shifted twice. Diagnostic system objective is to measure the scattered radiation. The magnitude of the shift reflects information about electron temperature T_e, whilst the measured intensity is proportional to electron density n_e. Typical temperatures achieved in plasma experimental devices range from units of eV to tens of keV.

Thomson scattering geometry and cross-section

From the calculation of radiated power of scattered light one can determine Thomson scattering *cross-section*, which has a relation to the probability of single scattering event. In general directional energy flux density of an electromagnetic field is represented by Poynting vector where the electric field generated by a moving charged particle is substituted. This field one can determine from Lienard-Wiechert potentials [20, p. 5]. Total radiated power is defined as the energy over time integrated over whole sphere. Carrying out the integration results in the equation (1.3), where q represents charge of the particle (electron charge) and $\gamma = 1/\sqrt{1-\beta^2}$, where $\vec{\beta} = \vec{v}/c$, other quantities can be recognized from Fig. 1.2a or defined above. Fig. 1.2a shows the scattering coordinate system. Light scattered by *particle* with the $\vec{v}$ speed at the *origin* is observed by the *Observer*. Vector $\dot{\vec{\beta}}$ refers to the acceleration of the particle given by the electric field $\vec{E}_i$ of the incoming electromagnetic wave.

$$P_{tot} = \frac{q^2\gamma^6}{6\pi c\varepsilon_0}\left[\dot{\beta}^2 - \left(\vec{\beta}\times\dot{\vec{\beta}}\right)^2\right] \tag{1.3}$$

Strong dependence on the γ factor indicates that an accelerated charged particle radiates strongly as its speed rises. Two basic situations can be distinguished depending on the orientation of vectors $\vec{\beta}$ and $\dot{\vec{\beta}}$. In both cases the accelerated particle emit in the direction of $\vec{\beta}$ more and more as its speed approaches the speed of light, referred to as *headlight effect*. High-speed electrons from the velocity distribution thus scatter more light in their motion direction, i.e. towards an observer. Electrons moving away from the observer will scatter very little portion of light in the direction of the observer. Consequently combination of these two effects will due to Doppler effect shift the peak of the spectrum of the scattered light towards the shorter wavelength, so called *blue-shift*. More information and detailed derivation of mentioned facts together with visualisation could be found in [20].

Thomson scattering cross section σ_{TS} is typically derived for low-temperature case when $\beta \ll 1$, $\gamma \equiv 1$. Total radiated power of Thomson scattering is then given as:

$$P_{tot} = \frac{8\pi}{3}\, r_e^2\, S_{inc} \tag{1.4}$$

where the quantity r_e is known as standard electron radius and S_{inc} denotes to the magnitude of instantaneous Poynting vector. The quantity of proportion between P_{tot} and S_{inc} is called

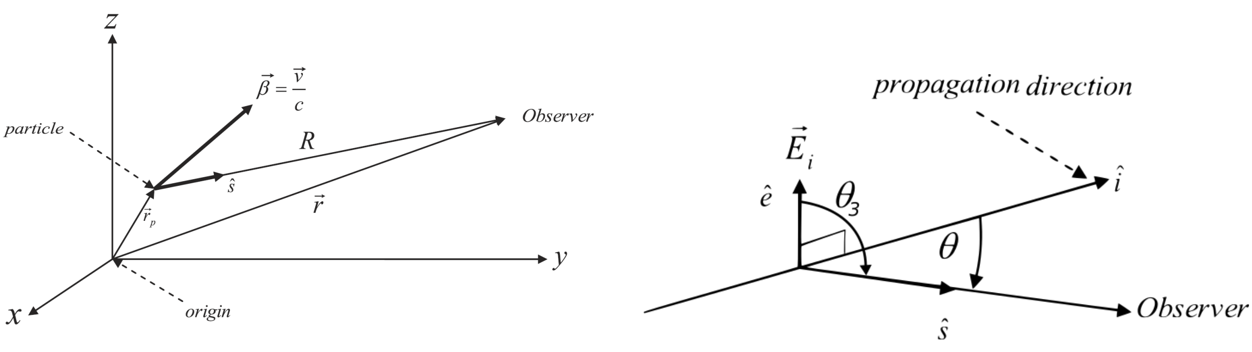

(a) (b)

Fig. 1.2: (a) Diagram showing the scattering coordinate system, (b) The incident electric field $\vec{E}_i$ is perpendicular to the scattering plane defined by unit vectors $\hat{s}$ and $\hat{\imath}$ [20]

Thomson scattering cross section σ_{TS} (1.5a) and it is very small, equal to $6.65\times10^{-29}\text{m}^2$. As a consequence only high intensity light sources enable using this diagnostic technique. Also σ_{TS} is inversely proportional to particle's mass squared, therefore electron scatter approximately 3.4×10^6 more power under same conditions [20, p. 14]. This makes Thomson scattering by ions negligible in contrast to the one induced by electrons.

$$(a) \quad \sigma_{TS} = \frac{8\pi}{3} r_e^2 \qquad\qquad (b) \quad \frac{\mathrm{d}\sigma}{\mathrm{d}\Omega} = r_e^2 \, \sin^2\theta_3 \tag{1.5}$$

Differential cross-section $\mathrm{d}\sigma/\mathrm{d}\Omega$ can be derived from equation for the power $\mathrm{d}P$ radiated per unit solid angle $\mathrm{d}\Omega$ using the same approximation. The result is shown in equation (1.5b), where θ_3 is the angle between $\vec{E}_i$ and $\hat{s}$ from the Fig. 1.2b. Differential cross sections shows the spatial distribution of scattered power. It is maximal when $\theta_3 = 90°$. Thomson scattering is therefore most effective in the plane perpendicular to $\vec{\beta}$, in other words in the plane of the polarization of the incident electromagnetic wave. Therefore polarizers are often used to select the desired polarization to ensure the highest efficiency of the diagnostic. For most cases linear polarization is used.

Spectrum of the scattered light

Last section is denoted to the derivation and discussion the spectrum of the scattered light. One can determine the spectrum from the scattering of incoming wave by a single electron, which is afterwards averaged over the ensemble of particles with characteristic velocity distribution. Stated before the scattering process strongly depends on particle (electron) velocity and considering that the particle energy within the high-temperature plasma might reach substantial portion of the speed of light, relativistic Maxwell-Boltzmann distribution $f_R(\vec{\beta})$ is assumed [20, p. 43].

Spectral function S giving the spectral distribution of the scattered radiation by a set of particles with chosen velocity distribution can be determined evaluating following integral

$$S = \int\int\int \left(\frac{\omega_s}{\omega_i}\right)^2 (1-\beta^2)\, f_R\left(\vec{\beta}\right) \delta\left(\vec{k}\cdot\vec{v} - \omega\right) \mathrm{d}^3\vec{\beta}, \tag{1.6}$$

where ω_s and ω_i represents the angular frequency of scattered and incoming (laser) light wave, respectively, and δ refers to Dirac delta function. During derivation of the expression (1.6) an approximation was made. A term, so called *depolarization term*, was neglected, due to the fact, that its effect is approximately constant in relevant wavelength range and has not negligible impact once the temperatures of 10 keV are exceeded. For illustration the Fig. 1.4 shows this term for standard TS configuration. It can be observed that for $T_e = 20\text{keV}$ the intensity reduction is approximately 7% and remains constant in ε range from -0.5 to 1.0.

Carrying out the integration for this situation results is the term (1.7). Previously not described quantities α, ε and x are given by (1.8), where λ_s and λ_i stands for wavelength of the scattered and incident (laser) light and angle θ is defined in Fig. 1.2b.

$$S(\varepsilon,\theta,2\alpha) = \frac{\exp(-2\alpha x)}{2K_2(2\alpha)(1+\varepsilon)^3}\left[2\,(1-\cos\theta)\,(1+\varepsilon)+\varepsilon^2\right]^{-1/2} \tag{1.7}$$

$$\alpha = \frac{m_0c^2}{2k_BT} \qquad \varepsilon = \frac{(\lambda_s-\lambda_i)}{\lambda_i} \qquad x = \left[1+\frac{\varepsilon^2}{2\,(1-\cos\theta)\,(1+\varepsilon)}\right]^{1/2} \tag{1.8}$$

Shape of the spectral function S is shown in Fig. 1.3 for temperature range from 1 to 20 keV, when only electrons are considered as a scattering medium, for 90° geometry diagnostic system. Shift of the peak position to shorter wavelength with rising temperatures (*blue-shift*) can be observed together with the broadening of the whole spectrum.

In principle, the aim of a diagnostic system based on Thomson scattering is to reconstruct the scattered spectrum from detected signal. Eventually spectrum width and shift of its peak leads to determination of electron temperature and the measured intensity is proportional to electron density.

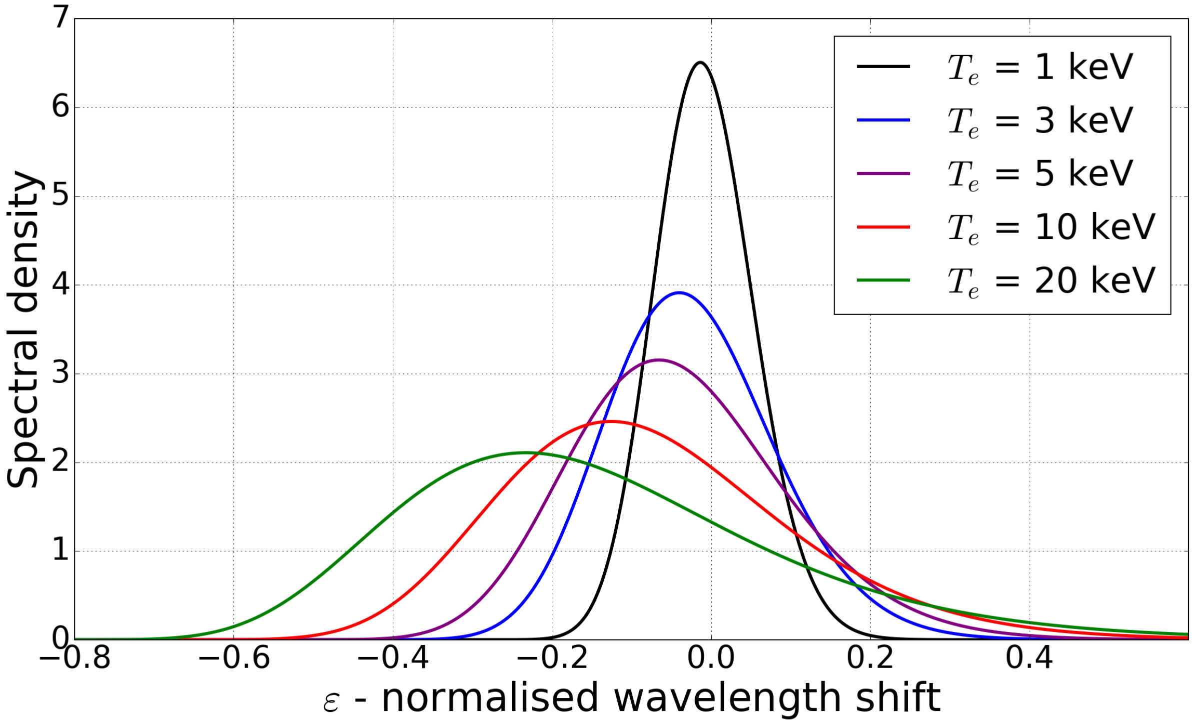

Fig. 1.3: Spectrum of the scattered light S as a function of ε for temperature range 1 - 20 keV for 90° geometry TS.

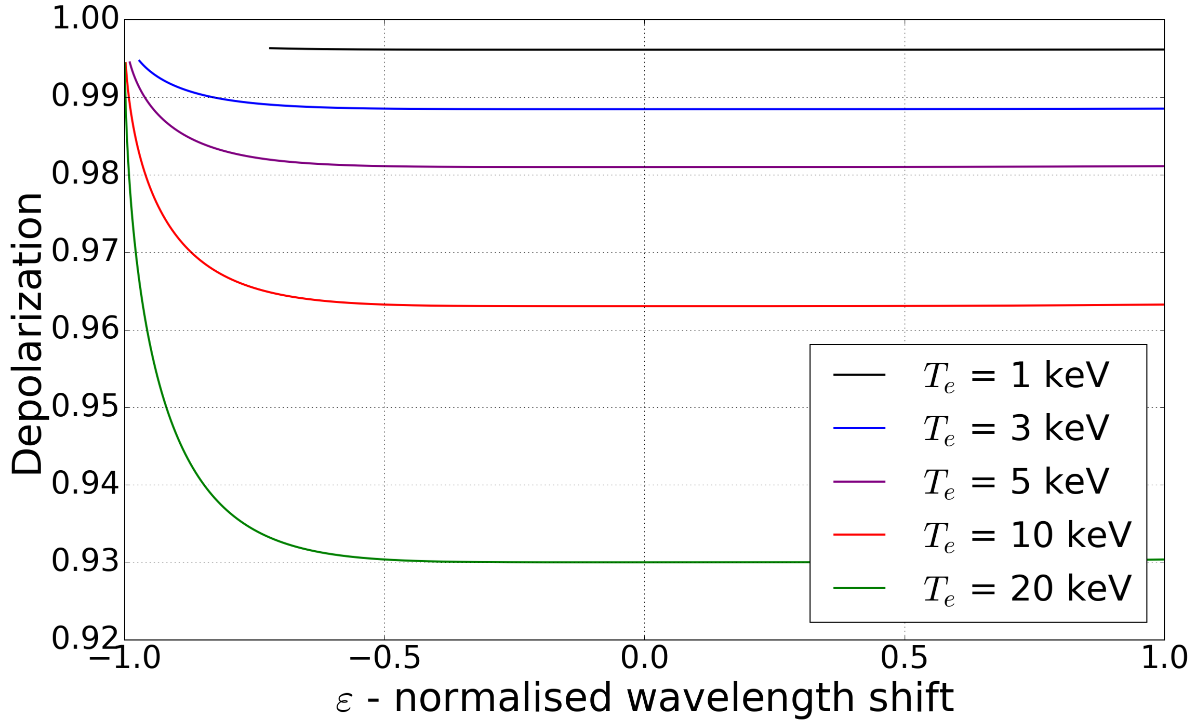

Fig. 1.4: The dependency of depolarization term on ε for temperature range 1 - 20 keV for 90° geometry TS.

Chapter 2

Thomson scattering diagnostic system on tokamak COMPASS

In general, it can be stated that diagnostic system based on Thomson scattering is very complex, complicated and susceptible to even delicate spatial or temporal inaccuracy. Due to the very low cross-section (1.5) value, TS diagnostics system becomes feasible once high-energy and high-power lasers as sources for probing electromagnetic wave are used. Despite this fact, low level intensity of scattered radiation is provided, which imply very high and strict requirements on components for light collection, transmission and detection. Appropriate configuration and proper adjustment of components together with high precision calibration routines are essential to provide reliable measurement of plasma parameters.

Thomson scattering diagnostic (TS) system on tokamak COMPASS is designed to measure electron temperature in range from 10 eV to 10 keV and electron density of optimally 10^{19} m^{-3}. Whole system is presented on the schematic figure Fig. 2.1, where the key components are shown, namely lasers, collection and transmission optics, detectors and data acquisition part. Following section is dedicated to mentioned components in more detailed manner.

2.1 Laser system

For the purposes of obtaining sufficient scattered light two independent high-power Nd:YAG lasers with energy 1.5 J and repetition rate of 30 Hz are installed at COMPASS tokamak facility. Three different regimes for lasers operation are implemented. Individual control enables triggering lasers both simultaneously in order to deliver twofold higher energy in single moment and separately resulting in either 60 Hz pulse frequency or a operation in so called *"burst regime"*, when the delay between two pulses can be optimised for the purposes of the experiment demands.

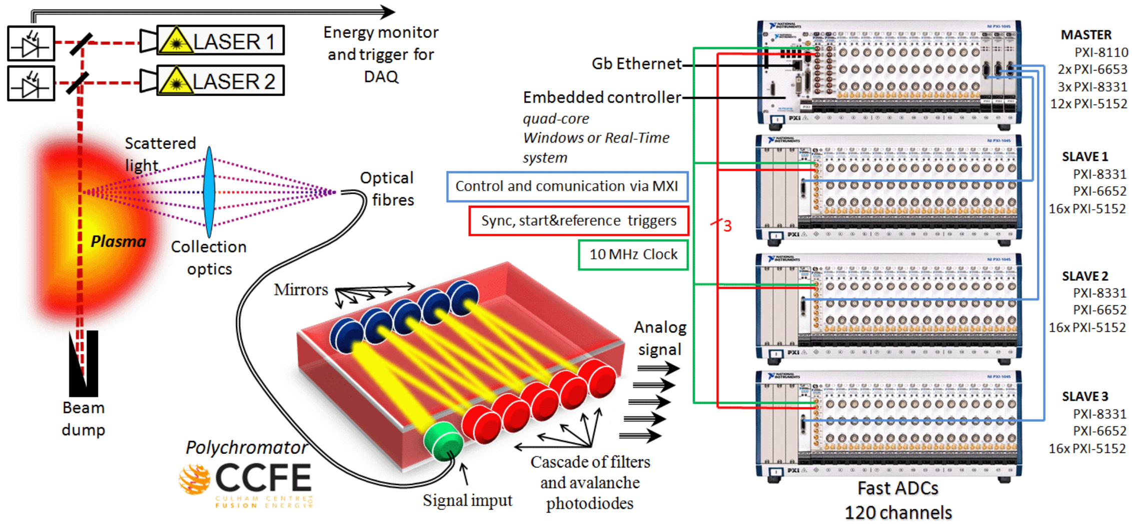

Fig. 2.1: Thomson scattering diagnostics scheme on tokamak COMPASS [14].

Both laser beams are led to the tokamak device by 20 m long enclosed path and enter tokamak vessel through vacuum window placed at Brewster angle to avoid unintentional reflections and through pipe with number of apertures to reduce stray light [4]. After leaving the plasma region remaining laser energy is absorbed by laser beam dump situated 2.48 m beneath the vessel to prevent undesirable back reflections of laser pulses [4]. In addition several diaphragms elements are placed to the laser beam path to achieve as high precision as possible together with high stray light mitigation, which is a key issue for the TS diagnostics. Anti-reflex coating od optical elements participating in scattered light collection and transmission improves stray light mitigation. Additional portion of stray light that comes from plasma background as a result of bremsstrahlung is reduced by the factor of two by polariser. [4]

2.2 Optical system

TS system is designed to view both plasma edge and centre with two collection objectives optimised for appropriate wave range. Region observed by core and edge diagnostic is pictured on Fig. 2.2a. Core objective observes centre and upper part of plasma along the vertical axis -30 mm to 210 mm over the mid-plane, with spatial resolution of 8.1 to 12.4 mm. Edge system was originally proposed to have a field of view from 200 to 300 mm over mid-plane, with spatial resolution up to 3 mm. In praxis, these specifications were not achieved, the covered range did not reach the plasma edge for all plasma scenarios, the resolution was degrading at the edge as well. Recent modulation of the view port allowed better coverage of the edge plasma region, extending the view beyond z = 300 mm, and improving the resolution. [results planned to be presented this year]

Scattered light is afterwards focused on transmission fibre bundles that corresponds to spatial points inside the tokamak vessel. In total the observable region is divided into 54 points, from which 24 belong to core TS while the rest to edge TS. Optical fibres made of polymer cladding silica are chosen due to favourable properties when operating with infra-red part of EM spectrum. Scattered light from two adjacent spatial points is led to one detection unit (described below) by fibres of a different length thus enabling reduction of detection units by a factor of two. This method, so called *duplexing*, is based on a time delay of collected signal, due to the different length of path to travel from a source to a detector. Furthermore several fibre bundles (2 core, 2 edge), called *"split fibres"*, have additional function that helps verifying correctness of measurement. Signal from one spatial point is focused on specific fibre bundle, which is vertically separated into halves. Then the scattered light is led to a single detector unit using duplexing method, and the intensity in both halves is compared to each other. Split fibre method is used as to control relative position of the probing laser beam and collection optics. One can easily observe that ideally the ratio of intensities equals to unity. In order to use split fibres to measure plasma parameters, signal in both halves is added together. Therefore one detection unit is necessary for one split fibre in contrast to other fibre bundles, where one detector is able to acquire data from two fibre bundles, thus two spatial points. Typical result of split fibre measurements is shown on Fig. 2.2b. [15, 17, 18]

2.3 Detection and data acquisition

Detection of spectral composition of scattered light collected by optical system is on COMPASS tokamak provided by means of 29 filter polychromators, that are the fourth generation detectors for the purpose of TS diagnostics developed on tokamak MAST, CCFE, UK [21, 22]. Generally, filter polychromator is a type of detector that enables spectral decomposition of incoming optical signal. Fig. 2.3a shows the basic scheme of a polychromator with seven filters. Input signal is reflected on the first interference filter which transmits certain narrow spectral range while the rest is reflected on second filter, and so forth. Thus each filter acquire different part of input signal, which is after passing through multiplied and detected by avalanche photodiodes (APD) to obtain sufficiently high intensity. Set of spectral filters, or channels, is designed in order to cover required wavelength range and to suppress unnecessary losses of useful signal. Five channel polychromator modification of shown detection unit is incorporated to TS system on COMPASS tokamak. Spectral transmittance of individual filters is presented on Fig. 2.3b, where one can easily observe the covered wavelength range with overlaps of filter transmittance to reduce potential losses.

Amplified signal exiting APD is eventually digitized by total count of 120 ADC[1] converters, whose set up is illustrated at Fig. 2.1 as Fast ADCs. Using high-pass filter with sampling frequency of 1GS/s in scale of 8bits digital output signal is obtained and afterwards saved and stored for following data processing and analysis. [17]

[1] ADC = analog-to-digital converter

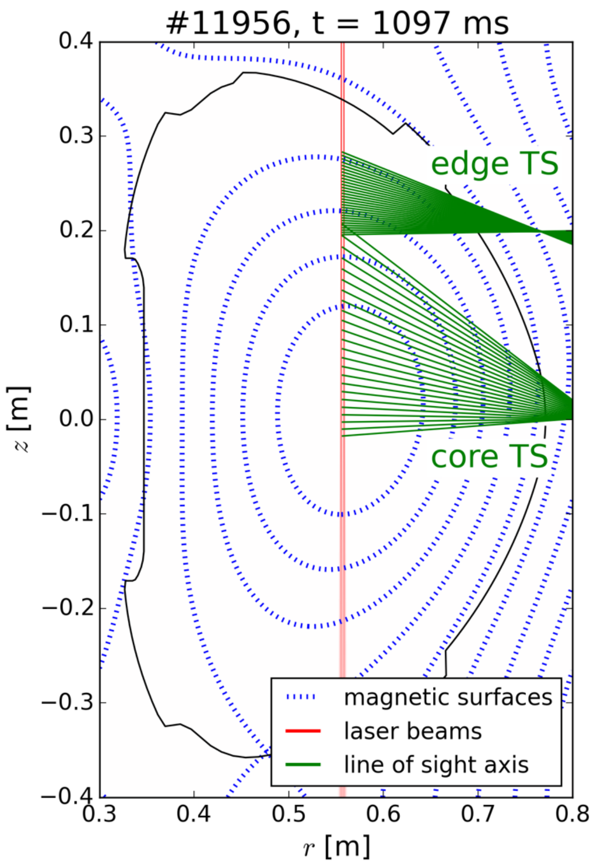

(a)

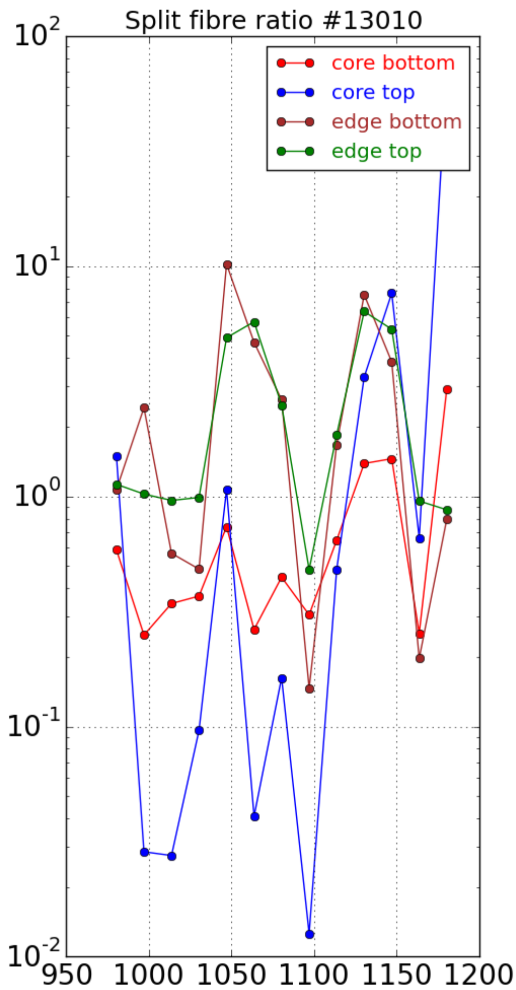

(b)

Fig. 2.2: (a) Observed plasma region by both core and edge TS diagnostic [16], (b) results from the split fibre method measurement for tokamak discharge #13010 on COMPASS, labels ”bottom” and ”top” signifies position inside the tokamak vessel of spatial point for ”core” or ”edge” system.

2.4 Data processing

The overall objective of data processing procedure is to reconstruct spectrum of the scattered light from collected signal by means of previously discussed components to determine plasma parameters, electron temperature and density. Data processing technique is similar to calibration routines described more in detail in [11] or [24, czech only], whose result is ratio of expected signal on two adjacent spectral filters (2. to 1. channel, 3. to 2., etc.) dependent on electron temperature. Resembling ratios can be calculated from detected signal and the key issue consists in fitting them to ones obtained during calibration routines. Detailed description of this process is one of contributions of this work and will be described below (see Section 4.2).

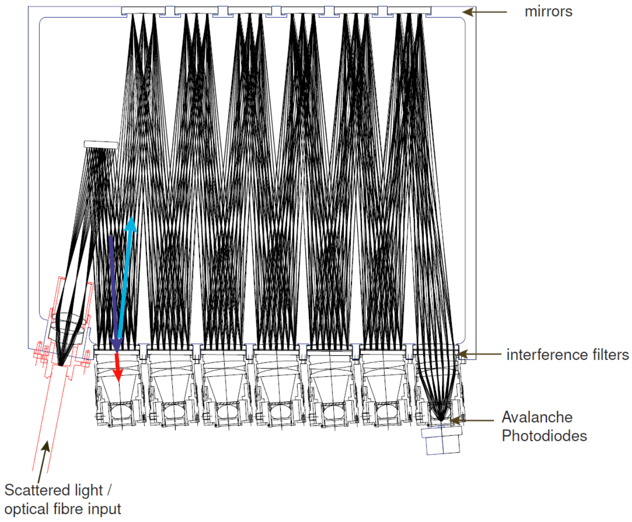

(a)

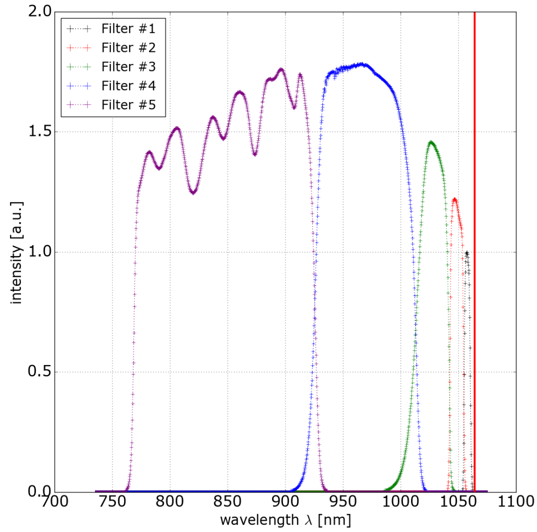

(b)

Fig. 2.3: (a) Scheme of filter polychromator used on tokamak MAST and COMPASS [23], (b) spectral transmittance of spectral filters for polychromator #523 on COMPASS, measured 19/11/2014 [24].

Chapter 3

Research study - alignment control

Following chapter consists of research study with relation to tasks from the assignment of this work or other relevant aspects.

3.1 Alignment control

First assignment task is concerning control of laser beam position by means of camera recording of the laser beam spot together with remotely operated motorised mirrors. Therefore techniques assisting proper alignment of the diagnostics especially laser position control is discussed in this section.

Precise alignment of the probing laser beam and collection optics are one of crucial aspects that determines the accuracy and reliability of TS measurement. Even slight misalignment might lead to extensive inaccuracies in plasma parameters determination or even might disable the measurement completely. For instance, in the case of scattering angle θ_3 from (1.5b) an error of $1°$ for $\theta_3 = 90°$ corresponds approximately with 2% error in electron temperature estimation [8]. The laser misalignment effect on determined electron density is even higher - the scattered light intensity loss is interpreted as lower density. Several methods employing different means are vastly used on experimental devices around the world in order to ensure proper adjustment of both laser beam path and collection optics which also might have significant influence on the measurement accuracy. In the sections below both issues are discussed.

3.1.1 Laser beam position

Basic laser beam position control method is usually done by the personnel on a daily basis as a visual control of the correct position of laser spot reflecting from imaging mirrors or on reference elements placed in the laser beam path. To avoid damaging the elements and possible harmful unintentional reflections or focusation of the probing laser beam, guiding laser or the same laser operated in significantly lower energy mode is used for the initial alignment control. Moreover, for diagnostic system using wavelength in the invisible region for human eye (typically infra-red), implementation of visible guiding laser is indispensable. More detailed, accurate and reproducible control can be performed by means of proper cameras which are set to view the laser spot on a mirror or on a shade screen behind. This technique is usually combined with positioned steering mirrors remotely manipulated by motorised actuators.

Chapter 4

Measurement description and results

Following chapter includes description of measurements, advancements and procedures performed or implemented within the framework of this research study. The author's aim is to show the methods as a process from its motivation to the implementation with proper testing and commissioning procedures being performed. Nevertheless various processes remain unfinished because rather suits as a preparation for establishing base with an expectant diploma thesis of the author.

4.1 Observation and correction of laser position

Mentioned above spatial calibration and laser beam alignment are essential issues that require major concern in order to provide reliable and precise measurement with diagnostics based on Thomson scattering. Various methods concerning this subject implemented on worldwide devices are presented in previous Chapter 3.

Thomson scattering diagnostics system on the COMPASS tokamak described in Chapter 2 accommodates two diagnostic (probing) Nd:YAG pulsed lasers operating in infra-red spectral region which share laser beam path leading from the laser room to the tokamak hall through the tokamak vessel along the vertical axis. Laser path is ended by a beam dump located 2.5 meters beneath the vessel [4]. Each probing laser is supplemented by a continuous tracing laser with a wavelength in visible spectral range (red colour). Outline of TS system including the laser beam path is presented in Fig. 4.1. One can see that the direction of laser beam is altered several times by appropriate mirrors before entering the vessel due to space and safety constraints.

Each optical element placed to the laser beam path represents a potential source of misalignment or might result in degradation of laser beam quality. Therefore proper control of the laser beam position when interacting with given optical element improves general performance of the diagnostics. Current situation of TS diagnostic system enables observation of the tracing

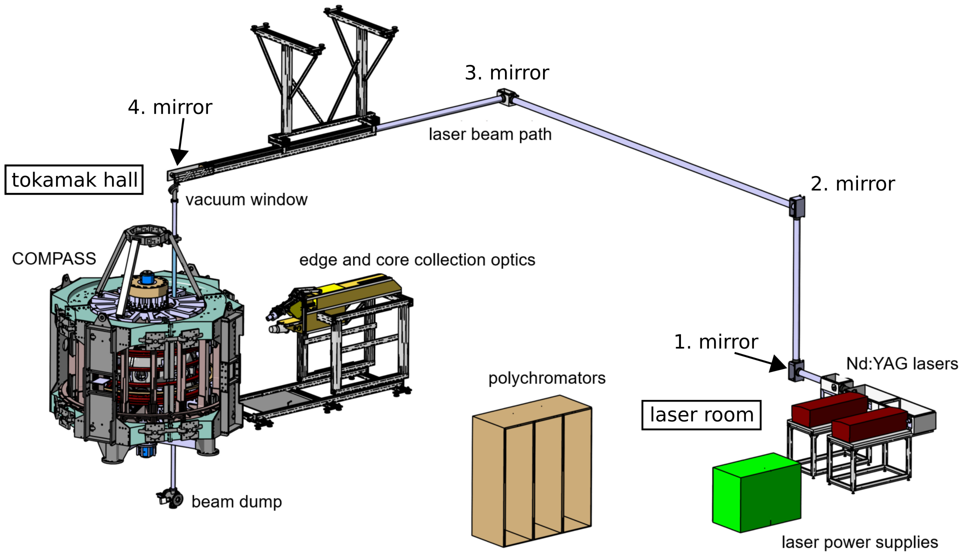

Fig. 4.1: Thomson scattering diagnostics system arrangement on the COMPASS tokamak [16].

laser spots on the 2. and 3. mirror in the path by means of IP cameras, which primarily serves as a control device during adjustment of the laser beam path when operating the diagnostics. In the initial phase of experiment operation the laser beam path is optimised based on the tracing laser spot position on a surface of reference components placed to the laser path.

Approach presented by this research study proposes laser beam control and adjustment by means of viewing laser spot on mirrors and recording its movement over time. For the purposes of altering the laser beam position, mirrors supposed to be manipulated by remotely controlled motorised actuators with precisely defined motion steps in order to provide as accurate adjustments as possible.

The intention consists in capturing images of the tracing laser spots during operation which are afterwards digitally processed in order to obtain laser position in relation to the one previously

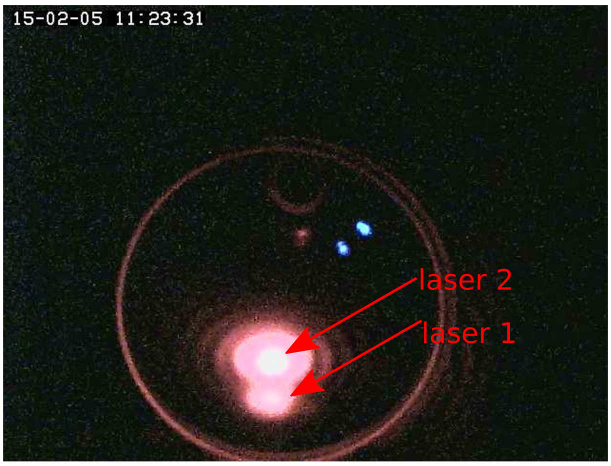

Fig. 4.2: Tracing laser spot (red spots) on the 3. mirror in Fig. 4.1.

measured. Based on acquired data appropriate corrections of a tilt of the observed reflective mirror will be computed and performed. To achieve high reliability of this technique a controlling mechanism is inevitable to be implemented.

4.1.1 Evaluation of proper camera

The realization of proposed project requires possession of components, especially adequate camera, which complies with requirements. Fundamental camera parameters, that were concerned, when deciding on proper model, are listed below:

- Resolution
- Frame rate
- Readout method
- Interface
- Cost
- Sensor type and size
- Colour space
- Pixel size
- Quantum efficiency (QE)
- Signal to noise ratio (SNR)
- Temporal dark noise (TDN)
- Saturation capacity (SC)

The most relevant parameters are *resolution, frame rate, cost* and *sensor quality* (not in order of importance), where sensor quality is evaluated using standard methods for sensor evaluation based on parameters in the right column, which is described below. Colour space was selected to be monochromatic, more precisely an image is shown in tones of grey.

Various monochromatic camera and sensor models were considered according to criteria in the left column with higher demands on mentioned parameters. Resolution of at least 1.5 mega pixels (MP) was required together with frame rate of at least 30 fps[1], due to the fact that the laser frequency equals 30 Hz, therefore recording the probing laser remains possible, although is not considered as a primary aim of this study. In order to capture laser beam pulse if necessary, the global shutter rather than rolling shutter readout method is required[2]. For the purposes of simplicity, convenience and versatility a USB interface was selected, namely USB3.

Two selected camera models fulfilling previous criteria are presented in Tab. 4.1. One can see that cameras significantly differ primarily in their quantum efficiency and saturation capacity. In order to perform more detailed camera comparison EMVA1288 imaging performance standard was used. The method follows white paper provided by FLIR (formerly PointGrey) Knowledge Base [2]. The procedure consists in three separate comparisons based on the theoretical amount of acquired signal with respect to noise.

According to the standard EMVA1288 signal can be computed using equation:

[1]fps - *frames per second*, which gives a maximum number of frames taken by a camera each second.
[2]Source: https://www.qimaging.com/ccdorscmos/pdfs/RollingvsGlobalShutter.pdf
[3]CMOS = Complementary Metal-Oxide-Semiconductor
[4]Unit e- represents the value equivalent to electrons. OTHER WORDS

	FL3-U3-20E4M-C	BFLY-U3-23S6M-C
Resolution	1600 x 1200 (2 MP)	1920 x 1200 (2.3 MP)
Frame rate	59 fps	47 fps
Sensor type	e2v EV76C5706F	Sony IMX249
Sensor size	1/1.8" (CMOS[3])	1/1.2" (CMOS)
Pixel size	4.5 µm	5.86 µm
QE (at 525 nm)	49 %	82 %
TDN[4]	21.53e-	17.31e-
SC	6018e-	32810e-

Tab. 4.1: General parameters of selected camera models. Data source: FLIR (formerly Point-Grey), https://www.ptgrey.com/, accessed: 3/2016

$$signal = light\_density \cdot (pixel\_size)^2 \cdot QE,$$

where the light density simulates the density of incident light on a sensor. An important assumption made at this stage is that the lenses have the same field of view, F-number and camera settings [2]. Proper lens selection and purchase is presented below. From the Fig. 4.3(a) one can see that BFLY-U3-23S6M-C (BlackFly) camera model generates higher signal at the same light density exposure and is also able to operate at wider range, almost to 1200 photons/µm^2, while the model FL3-U3-20E4M-C (Flea3) becomes saturated at the value of 600 photons/µm^2, as a result of almost fivefold higher saturation capacity together with better quantum efficiency despite 30% larger pixels.

For the application of this camera a low level light exposure is expected (laser spot in the dark laser path) therefore low level light density comparison when a noise becomes particularly relevant. Noise is estimated as a root mean square of Temporal dark noise and Shot noise equal to the square root of signal caused by nature of light:

$$noise = \sqrt{(TDN)^2 + (shot\_noise)^2}$$

The Fig. 4.3(b) shows calculated signal end noise. One can see that for low level light density noise level of BlackFly camera is slightly lower than for Flea3. For densities higher than 15 photons/µm^2 BlackFly's noise level exceeds the one of Flea3 (not shown in the figure), which is evident due to significantly higher signal for that range, as seen in Fig. 4.3(a). In addition it proves that absolute sensitivity threshold (the light level at which signal is equal to the noise) occurs at more than four times lower level of light exposure for the BlackFly model, which is favourable for camera application.

The more important measure needed to determine which camera will perform better in low light applications is the signal to noise ratio (SNR) [2], which si shown at Fig. 4.3(c). Theory suggests that higher SNR of BlackFly camera at low light density level implies better performance.

Based on accomplished comparisons that all individually acknowledge better performance of BlackFly camera, when even the its lower cost was taken into the consideration, BFLY-U3-23S6M-C model was purchased, with awareness of that the ultimate performance test is in the actual application. The fact, that Flea3 cost is higher than BlackFly model, is compensated by other features and functionality provided by drivers, which are not relevant for this application.

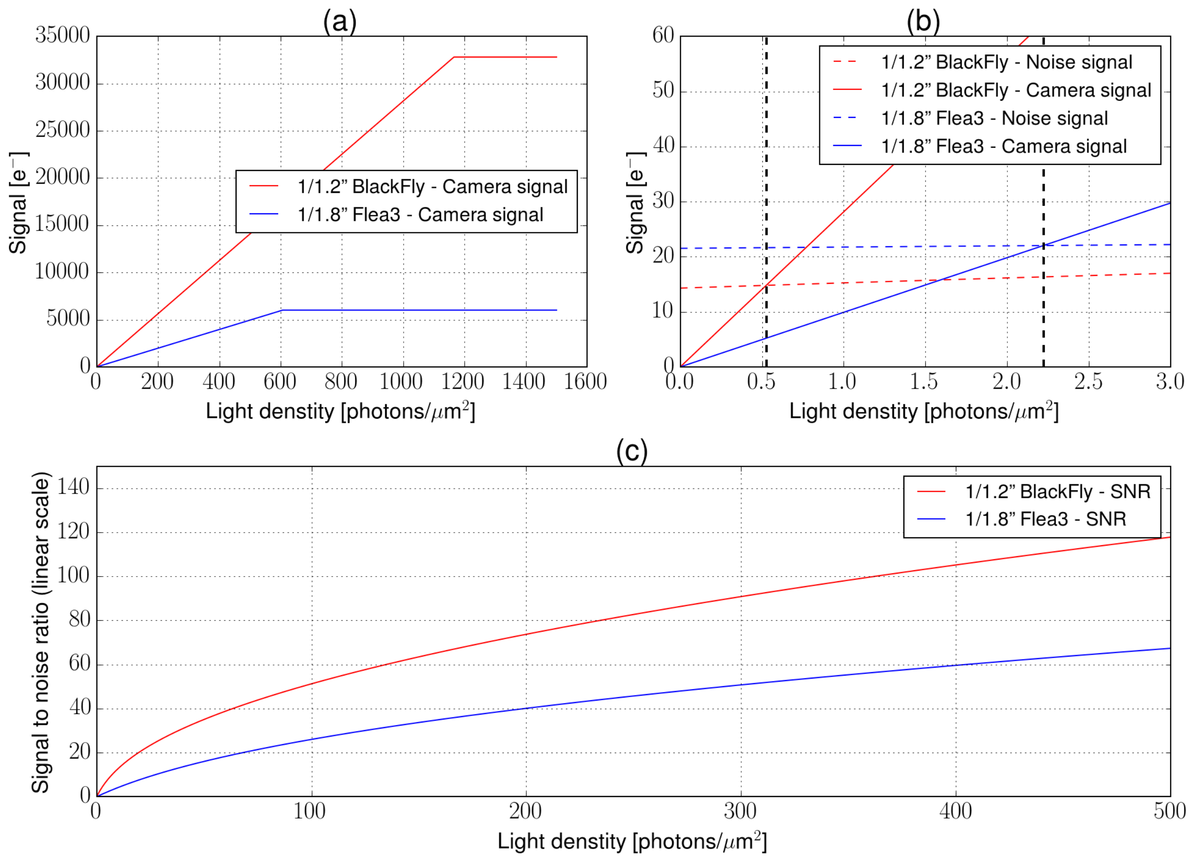

Fig. 4.3: Selected camera (BlackFly, Flea3) comparison. Figure (a) shows obtained signal as a function of light density, (b) compare the same signal to calculated noise and (c) show signal to noise ratio (SNR).

Lens selection

To complete and improve field of view of the camera and in general its operation capabilities a proper lens was decided to be purchased. When choosing a lens several aspects must be taken into consideration, the most relevant are *lens mount*, *lens focal length*, *sensor size* and *sensor spatial resolution* [3].

Most cameras are usually equipped by either C- or CS-mount, which vary in flange back distance and are incompatible with each other. Selected BlackFly camera is mounted by a C-mount therefore a C-mount lens supposed to be selected in order to avoid purchasing adapter components.

Another important aspect when selecting a lens is its focal length, that has the capability of changing cameras field of view. A lens focal length approximately equal to the diagonal size of the sensor reproduces an image similar to human eye perspective. Lenses with smaller focal length can be used to expand field of view unlike lenses with longer focal length that capture smaller field of view. Desired focal length can be calculated according to equation [3]:

$$focal\_length = \frac{sensor\_size \times working\_distance}{field\_of\_view + sensor\_size},$$

where the meaning of involved quantities are shown in the Fig. 4.4. Even if the camera application is not precisely defined, the previous equation can be used in order to estimate *focal_length*. Selected camera sensor (1/1.2") has dimensions of (10.1 mm$\times$ 8.8 mm) that is 13.4 mm diagonally. Proposed application suggests that working distance ranges from 10 to 15 cm while field of view takes a value of approximately 10 cm. Therefore calculated focal length ranges from 9.2 mm to 13.8 mm.

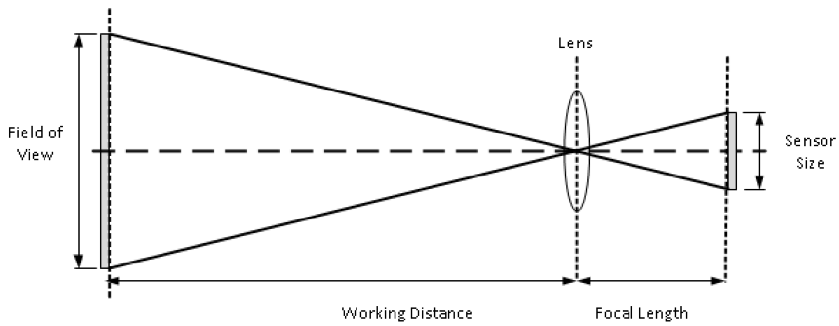

Fig. 4.4: Scheme showing relevant lens parameters [3].

On the basis of previous calculations and taking into consideration compatibility of the lens and sensor size together with its resolution a lens model **Fujinon F12.5HA-1™** with the focal_length of 12.5 mm was selected for purchasing.

4.1.2 Camera testing and basic operation

As stated above, this project is planned to be used as a tool for monitoring and controlling the laser beam to supply adjusting precise alignment. In general the camera observes tracing laser spot on a mirror in the laser beam path, that is placed in a mount equipped with position actuators. When operating, images are recorded and saved to be processed subsequently. From obtained images a laser beam position and its deflection from a reference (zero) state is calculated. The algorithm for mirror tilting actuators will be designed to correct eventual misalignment.

The scheme of the system is shown in the picture 4.5, where one can see a camera mounted with a lens observing an area of mirror in a holder equipped with one actuator for illustration. Two lasers produced laser spots are visible on a mirror surface.

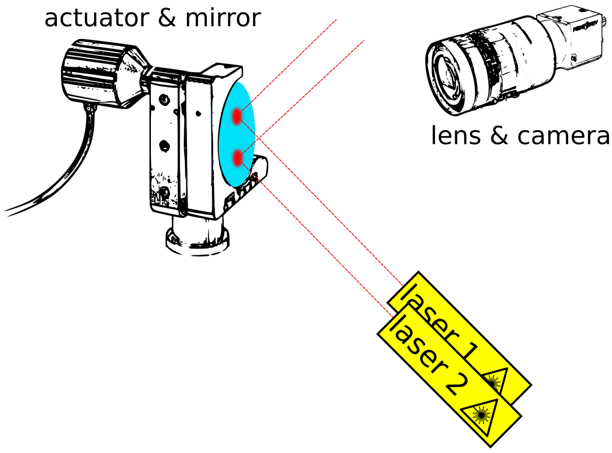

Fig. 4.5: Scheme of proposed mirror position control system.

The camera mounted with lens was successfully tested using a software tool called The FlyCapture Software Development Kit (SDK) supplied by the FLIR (formerly PointGrey) company. SDK software provides an interface to control and acquire images from various types of camera using the same API[5]. Good quality pictures were obtained. To illustrate one example picture of a mirror with two tracing laser spots is shown in Fig. 4.6. The improvement in comparison to IP cameras shown in Fig. 4.2 is significant. The resolution and frame rate was proven to be more than sufficient for proposed application, while the imaging and focusing capability of the lens are also satisfactory. Imaging device was also successfully tested in the near infra-red spectral (NIR) region, using a LED diode operating with the wavelength 940 nm.

SDK provides manifold options when considering a programming language for developing a new application, however, at the time of camera purchase it did not support Python as a tool for testing and development. Due to the author's custom and skills in using Python as a tool for programming and development the progress was suspended and for that time the effort was concentrated on the second main topic of this study. Nevertheless, future plans are described in the following section.

[5] Application Programming Interface - tool for building an application software.

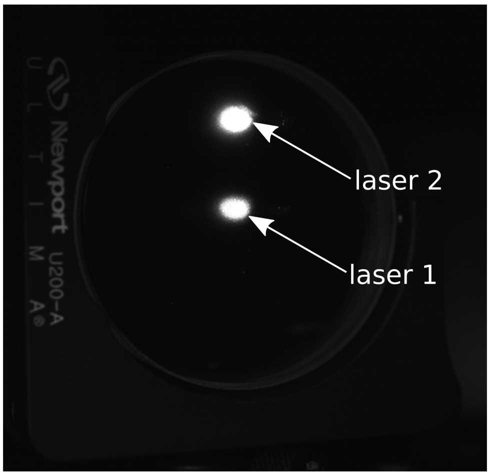

Fig. 4.6: Picture illustrating performance of purchased BlackFly camera on one of mirrors in the laser path. White dots are tracing laser spot shown in Fig. 4.5.

4.1.3 New SDK release and plans for the future

In the beginning of the year 2017 an updated version of SDK was released where, in addition to other upgrades, Python should be supported. Until now the beta version is still in the process of testing and debugging, on which author was invited by the manufacturer to participate.

The development of proposed laser position controlling system becomes feasible as the author is skilled in Python programming. The plan is to develop an algorithm, using the mentioned SDK, which will initially set-up the camera, then launch the observation of the tracing laser position with reference to the ideal one for which the system is designed to achieve as precise measurement as possible. The process of approaching the ideal position will be optimised in order to avoid oscillation around the optimal laser spot position. Each motorised device is characterised by the smallest possible movement or step, which sets the threshold fot precision of the alignment. Moreover, laser spot will be observed during the position adjustment and progress will be controlled.

Fig. 4.7 shows initial scheme of the algorithm when one camera and an actuator is used and laser alignment is being corrected according to one reference point. The ideal position is in this case defined by one point in space. Firstly an initialization process is performed to check if the system is operating properly, then last stable position and ideal position are loaded. The following loop is the core of the adjustment process when the laser spot is observed and the picture is saved, when not visible, a manual check by the personal seems to be required. Afterwards laser position is evaluated from saved picture and is compared with ideal state. In the case when there is a difference larger than given, threshold discussed above, the process of calculating mirror shift and performing proposed movement is launched. In order to mitigate oscillations around the ideal position, caused by a possible overshoot, only a portion of proposed mirror tilting is executed. The employment of this method into the algorithm requires testing procedures to be performed.

Realistic application on the COMPASS tokamak is affected by technical and spatial constraints. In general all mirrors have to be adjusted so that the required position of the laser beam within the tokamak vessel is achieved. One can see that it has to be defined by a vertical line connecting two points laser spots on the 4. mirror and beam dump. From Fig. 4.1 one can see that the 4. mirror in the laser beam path is located above the tokamak vessel and therefore it is ideal for adjusting laser beam inside the vessel. Unfortunately it is close enough to be influenced by magnetic field generated by coils during the tokamak discharge, that could produce undesirable effects due to the fact that proposed actuators function is based on electromagnetically driven stepper motor.

At this stage the position of camera and actuators is not certain and is planned to be designed and tested. Current idea is to place actuators on mirrors 2. and 3. due to their complicated access to and place the camera to observe 4. mirror and a pattern on a retractable beam dump. It means it can be moved away from beam path during alignment with tracking lasers, the laser spot is observable through a vacuum window behind the beam dump. In this situation, when at least one actuator and a camera do not manage same position, the issue becomes more complicated and more-dimensional then the one suggested to be solved by algorithm shown in Fig. 4.7. An iterative solution is planned to be proposed.

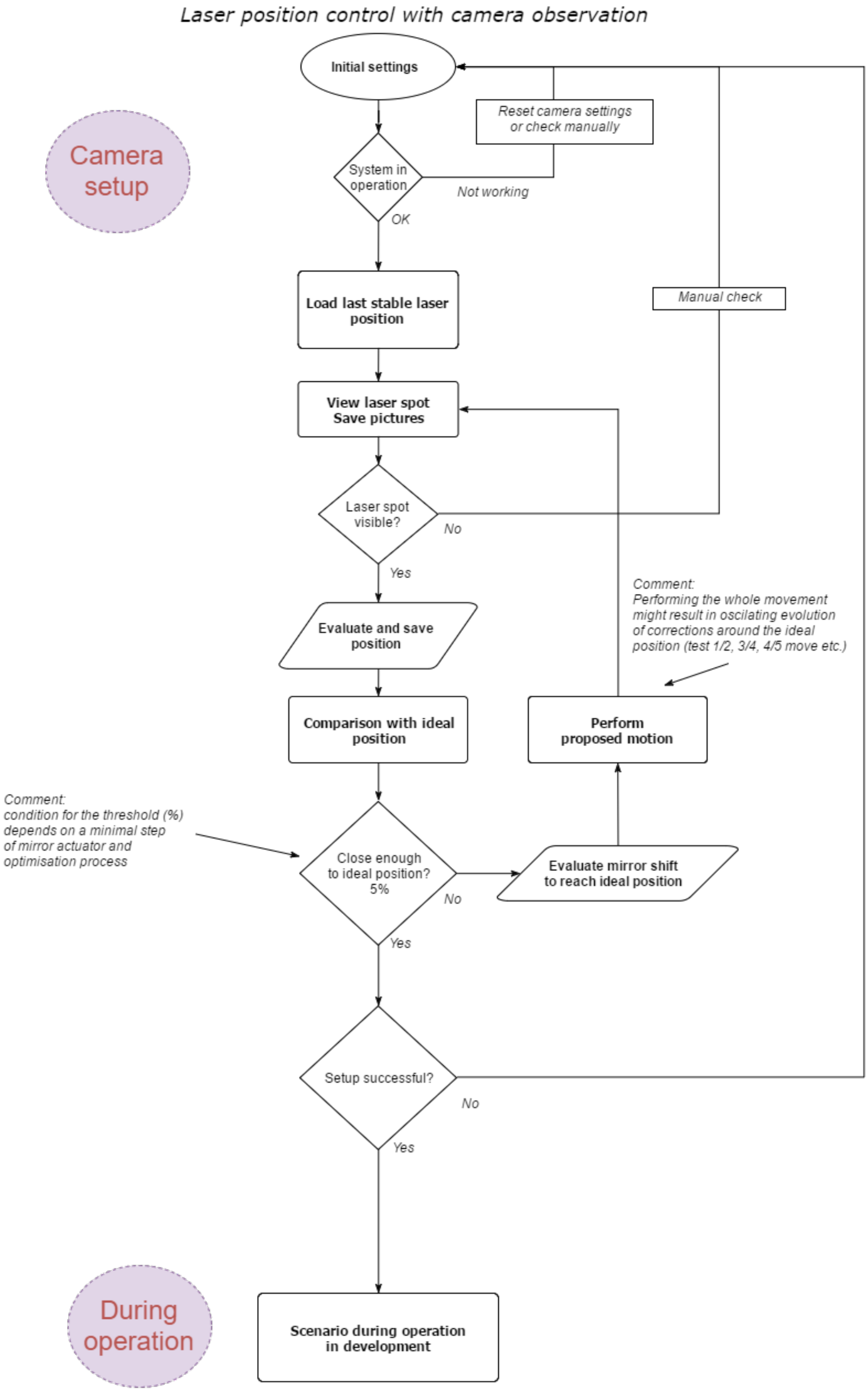

Fig. 4.7: Flow chart of proposed algorithm for camera control of laser position.

4.2 Data processing system

Following chapter describes data processing system of Thomson scattering diagnostics on the COMPASS tokamak. The issue of signal collection, detection and data acquisition is covered in Chapter 2. As mentioned in the Section 2.4, the main objective of data processing procedures is to reconstruct spectrum of the scattered light.

As stated in the Section 2.3, scattered light is collected by collection optical elements and transmitted by optical fibres to detectors. TS system on COMPASS is using a duplexing technique that enables detection of signal from two separate points within the tokamak vessel by a single detection unit (polychromator). Detectors operation is more precisely described in [4, 23, 24], and for the purposes of this work the key aspect is that transmitted signal is detected by five spectral channels, that are designed for detection of useful spectral region (750 to 1064 nm). At this moment, data from four spectral channels are digitised and recorded, due to the limited number of available digitisers. Demonstration of standard acquired raw data are presented in Fig. 4.8, where one can see fast component of detected signal (high-pass filter in the amplifier) by APD for all four spectral channels of four different polychromators, 504, 510, 520 and 528. Spectral channels numbering corresponds to the one presented at Fig. 2.3b. The graph on the right hand side shows spatial position at tokamak z-axis along the laser beam path (vertical direction) inside the vessel observed by given polychromators. Therefore, position $z = 0.0$ m refers to horizontal tokamak axis, called *midplane*. It is noted, that the area from which each polychromator detect signal has a shape of a rectangle due to rectangular arrangement of fibre bundles [17] and is only represented by its middle point in the figure.

When compared to Fig. 2.2a, core and edge TS diagnostic system are easily distinguished, blue dots signify edge while green core TS system. Number given after polychromator number (e.g. 510) specifies whether this position refers to the first (1) or to the second (2) peak shown at the left side in the same figure. This effect is a result of the duplexing technique, mentioned in section 2.2, that means that signal from two adjacent spatial points is driven to one detection unit with optical fibres of a different length (13 m), thus causing time delay of approximately 66 ns, when the refractive index of optical fibre is taken into consideration. To verify, it can be seen that the first peak has a maximum at approximately 620 ns and the second highest peak is located at roughly 685 ns.

The intensity of the signal is proportional to determined electron density, in general the higher the plasma density, the higher the intensity. Temperature determination is more complicated and is more precisely described at the end of this section. From Fig. 4.8 one can see the variance of signal intensity between both channels and polychromators themselves. For instance, in plasma core region higher temperature and density is expected, that correspond to stronger signal for polychromators 510 and 504, that observe this region. On the contrary, polychromator 520 observing plasma edge registers not negligible signal only in first channel, that signifies low temperature and density. This is evident from Fig. 1.3, since the closer the spectrum is to the probing laser wavelength the lower temperature is determined.

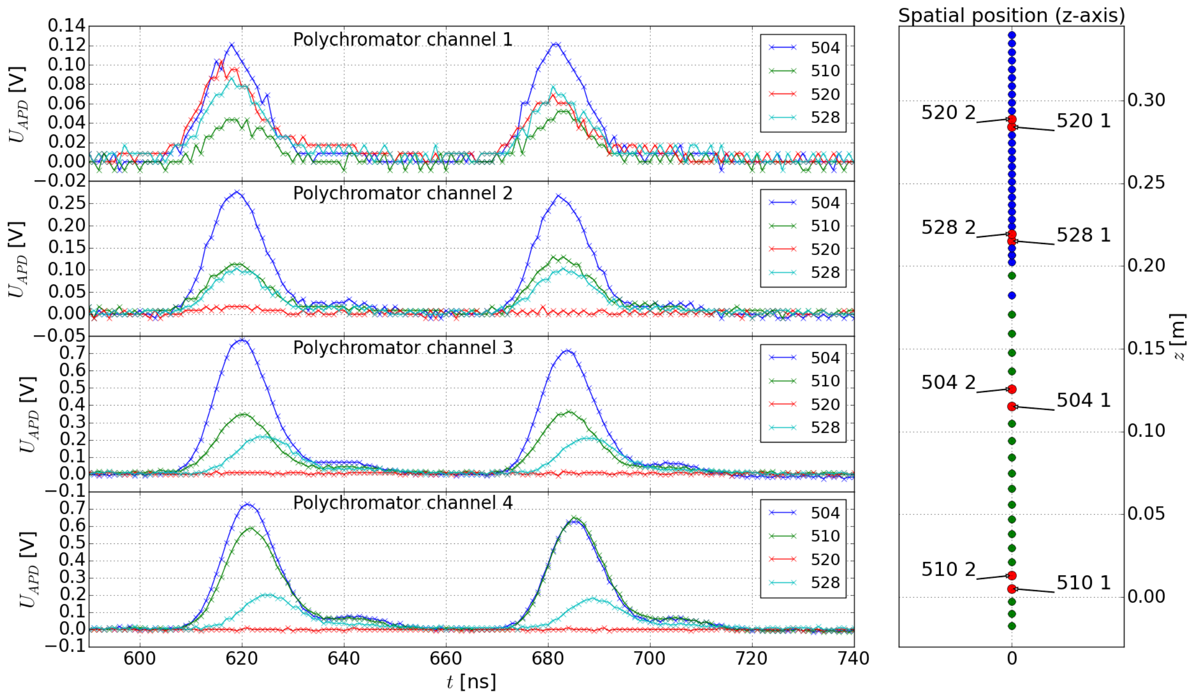

Fig. 4.8: Raw data acquired by TS diagnostic system. Data from 4 spectral channels shown for polychromators 504, 510, 520 and 528 for tokamak shot number #13007 for the same laser pulse inducing TS in flat-top phase when the current is constant.

It is observed, that each detected TS signal peak is followed by a second peak with variable but usually lower intensity, approximately one tenth of the first peak. It is assumed that this second peak is related to stray light and might impact determined electron temperature and density. This phenomenon is discussed below, together with different peak positions for polychromators evident from the graphs for channels 3 and 4.

4.3 Data processing algorithm

Up to the present day, data processing unit is based on routines received from Thomson scattering team on the MAST tokamak, when the COMPASS diagnostic was being put into operation. Processing system, provided in IDL programming language, was adjusted to fit hardware components and arrangement of COMPASS diagnostics and operation. Current approach in data processing development aims to the system review and design and implementation of a new system written in Python.

Overall flow chart representing TS data acquisition and processing together with indispensable calibrations that must be included is depicted in 4.9. Box on left hand side is devoted to issues connected with calibrations, while the right upper part labelled **Hardware** represents data acquisition part where a triggering unit is indicated. Right hand side box marked as **Processing** is mostly devoted to data processing itself, where spatial calibration section is included for the purposes of methodology conservation. Each part of the process will be described separately and afterwards their overall combination in order to produce proper results.

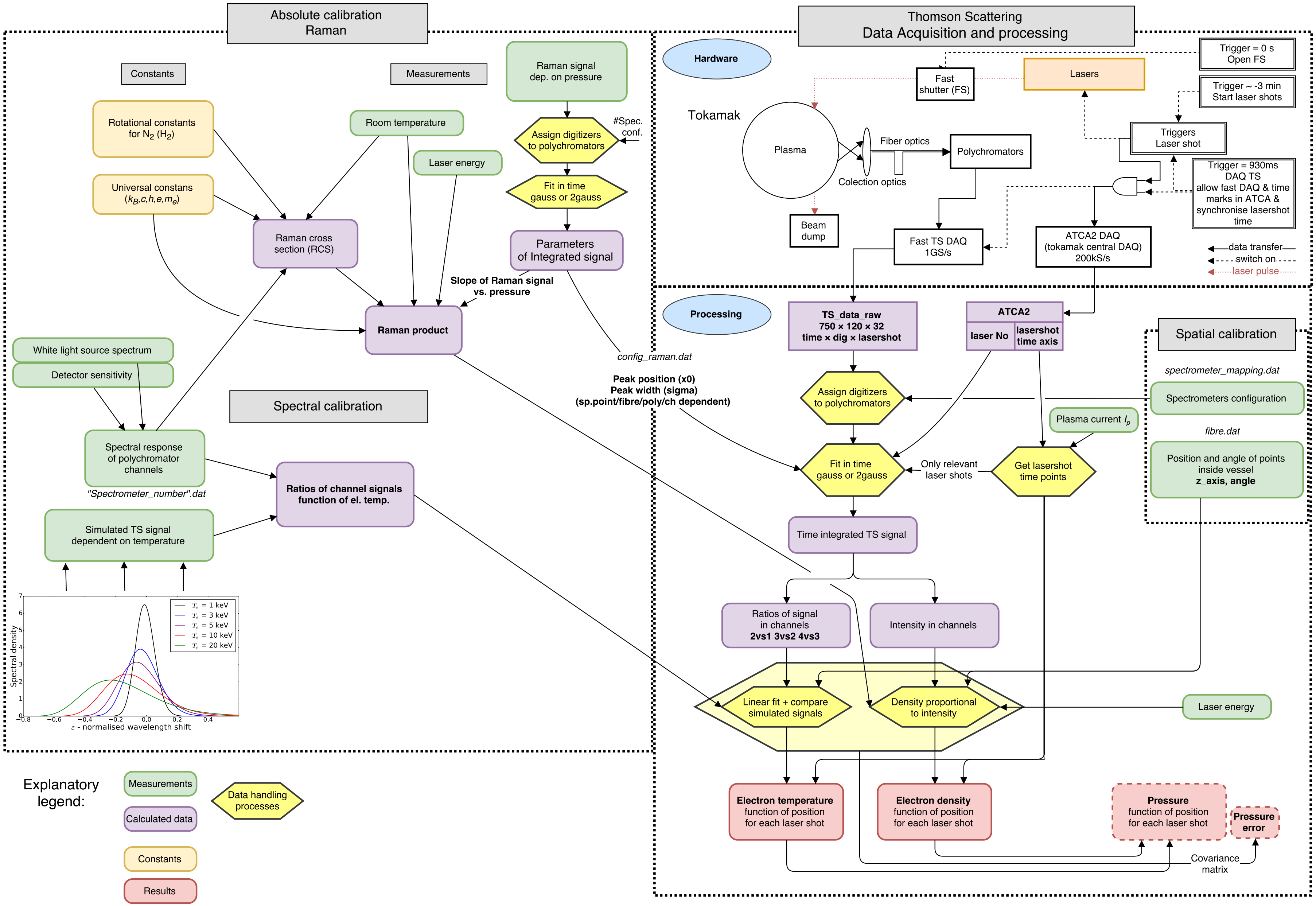

Fig. 4.9: Diagram showing data processing system for TS diagnostics on the COMPASS tokamak, further description in text.

4.3.1 Hardware part

Data acquisition part of the process is extensively described in [4, 11], therefore in this study it is covered briefly, but with strong emphasis on triggering system. Triggering system is responsible for precise synchronisation of successful progress of each tokamak discharge starting indispensable systems (power sources, plasma controlling systems, etc.) together with full synchronisation of diagnostic apparatus and data acquisition.

Triggering system for TS provides several functions [4]:

- laser operation
- synchronisation of lasers with each other - delay between pulses
- synchronisation to tokamak timing
- synchronisation of ADCs - for each laser
- operation of data acquisition system during plasma discharge

Each laser has two trigger inputs, one for flash lamps, that serves as a pump for a laser crystal, and one for operating Q-switching, both in 30 Hz regime. But when turning on the laser, achieving thermal equilibrium of laser optics (crystal) is important in order to ensure optimal parameters, i.e. energy, beam profile and divergence, therefore a preparation sequence for flash lamps is initiated by a trigger arriving at -3 minutes before the zero tokamak time, ensuring the lasers are at full power before the plasma discharge. At tokamak time 0 s fast shutter (FS) for laser beam is opened using another trigger signal. Usually, the tokamak discharge sequence is designed so that plasma is created at approximately $t = 960$ ms. Data acquisition (in graph DAQ TS) must be synchronised with laser pulses, more precisely, with the time of measurement of the respective laser pulse. For this purposes trigger at 930 ms is used for initialization. Since this moment, triggers are both triggering laser firing pulses to the tokamak vessel and copied to the tokamak data acquisition storage unit called ATCA2 DAQ, where the signals are digitised with 200kS/s sampling frequency. Moreover, for the purposes of synchronisation the same triggers are transmitted to fast TS data acquisition units, where the acquisition process is initialised this way. Laser beams are simultaneously travelling along their path towards the vessel and through the plasma, causing the generation of Thomson scattering signal, which is collected and detected by polychromators. Using fast ADCs the signal is digitised with sampling frequency 1GB/s.

Direct output of the DAQ system entering the processing part composes of two datasets, one containing Thomson scattering raw signals with specified dimensions, e.g. ($750\times120\times32$) at that time, that correspond to time series in nanoseconds (ns), a number of digitisers and a number of laser shots respectively, and second with time marks of the respective laser shot.

4.3.2 The process of calibration

Additional data inputs necessary for the calculation are result of various calibration routines.

Spectral calibration

Spectral calibration described in [11, 24] serves as a tool to calibrate spectral sensitivity of detectors using source of tunable monochromatic light and recording detected signal by each spectral channel. Corrections on detector sensitivity and spectrum of the white light source must be taken into account. Combined with simulated TS signal (see Fig. 1.3) dependent on electron temperature, ratios of channel signals as a function of electron temperature are calculated. Resulting data are stored in calibration files *"Spectrometer_number".dat* (e.g. *523.dat*) for each polychromator.

Spatial calibration

is another part of calibration process essential in order to achieve reliable measurements by any optical diagnostic system (section in right middle of the diagram). For TS system on the COMPASS tokamak it consists in providing file *fibre.dat*, that contains information about polychromators and digitisers settings together with position of each observed spatial point inside the tokamak vessel with reference to the optical system, namely their **z_axis** and scattering **angle** between the laser beam axis and line of sight.

Absolute calibration

Absolute calibration of TS system on the COMPASS tokamak is performed by means of rotational Raman scattering in nitrogen gas, whose theoretical principles are covered in section **??**. Absolute calibration of the diagnostic system should be provided on a regular basis to control its condition. The process could be divided in two stages. At first the value called *Raman cross section (RCS)* is computed as a product of Raman lines and spectral sensitivity integrated over the Raman scattering spectrum of a proper channel obtained by spectral calibration, see upper part of Fig. 4.10 or Fig. 2.3b. Since the laser wavelength is 1064 nm and the polychromators transmits only signal shifted towards lower wavelength, only anti-Stokes lines for N_2 are considered. Intensities are calculated according to (**??**) requiring gas molecule rotational constants and universal physics constants. Normalised lines are shown in the upper part of Fig. 4.10. The lower part of Fig. 4.10 shows the portion of Raman signal to given spectral channel of the polychromator 523. Values in the legend represents RCS. Identical calculation is performed for all polychromators and results for the first two spectral channels is displayed in Fig. 4.11.

For the second stage, i.e. computation of so-called *Raman product*, performing experimental measurement of Raman scattering is required. Tokamak vessel is filled with proper gas, nitrogen on the COMPASS tokamak, at measured room temperature T_R. Detected signal of Raman scattering induced by laser pulse of energy E_l is recorded, while the pressure of internal gas is decreasing. Number of records for each pressure and each laser is set high enough to provide sufficient statistics. On the COMPASS tokamak 60 records are performed. Averaging over valid

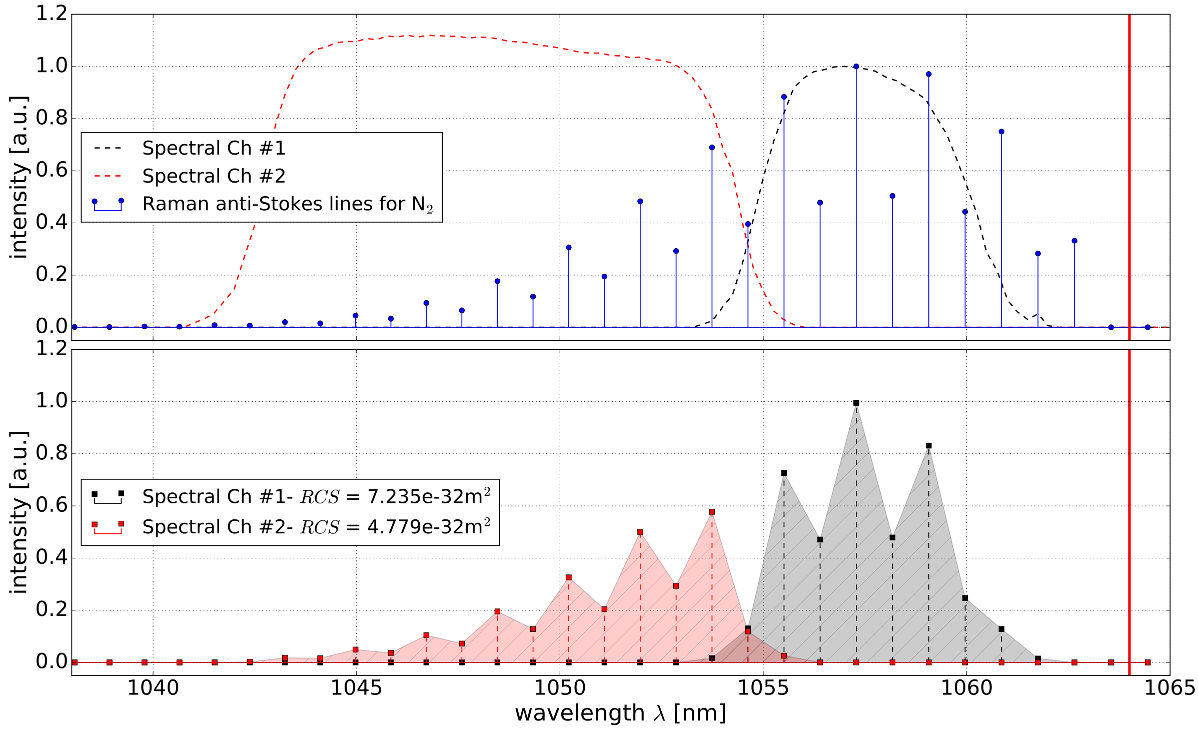

Fig. 4.10: Scheme for RCS calculation. Upper part shows normalised anti-Stokes Raman scattering lines in N_2 and spectral response of the first two spectral channels of polychromator 523, normalised to the maximum of the first channel. Lower part shows portion of scattered light belonging to corresponding spectral channel, where only discrete values are considered. Filling colour is displayed only for highlighting purpose. Value *RCS* represents the Raman cross section for given spectral channel. Laser wavelength is signified by red line on the right, 1064 nm.

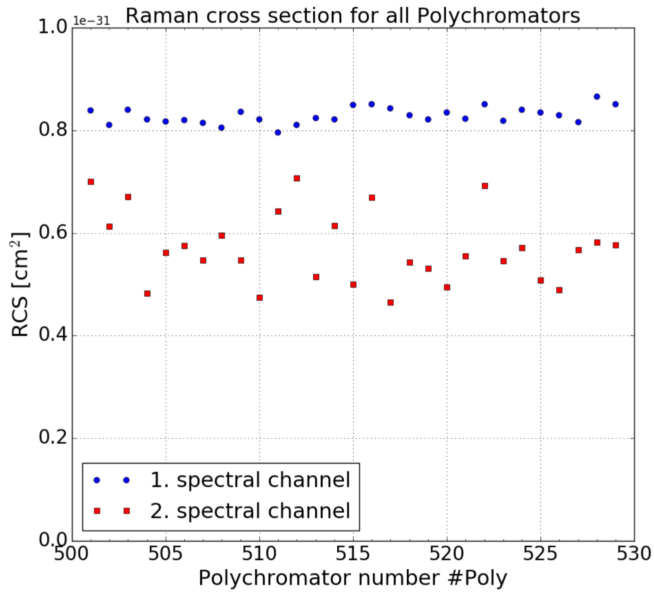

Fig. 4.11: Computed RCS for first two spectral channels of all polychromators.

records is included in the post processing process. Laser energy E_l is supposed to be monitored and recorded routinely. Raman product $R(i)$ for polychromator i is computed using equation

$$R(i) = T_R k_B \frac{r_e^2}{RCS(i)} \frac{k(i)}{E_l}, \tag{4.1}$$

where k_B and r_e refers to Boltzmann constant and classical electron radius, respectively. According to the theory, integrated signal of Raman scattering suppose to have a linear dependence on gas pressure and $k(i)$ signifies the slope of its linear fit, thus including the absolute transmission of the whole optical system. To assign detected signal from digitisers to the proper polychromator the *spectrometer_mapping.dat* file is used (signified by @Spec.conf.). Process of fitting and integrating acquired Raman signal with each individual laser shot in time is the same as for standard Thomson scattering and therefore is described in section (4.3.3) devoted to proposed data processing routine for TS. Typical integrated signal acquired by two first spectral channels of polychromator 506 is shown in Fig. 4.12a together with linear fit. Relative error of the shown fits is less then 0.5%, which is negligible in comparison to other error sources. Issue of errors is discussed afterwards.

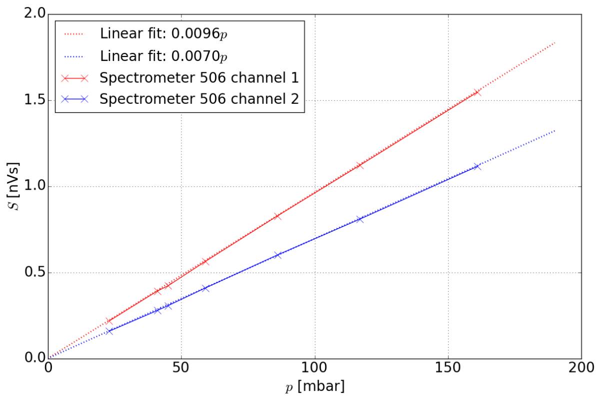

(a)

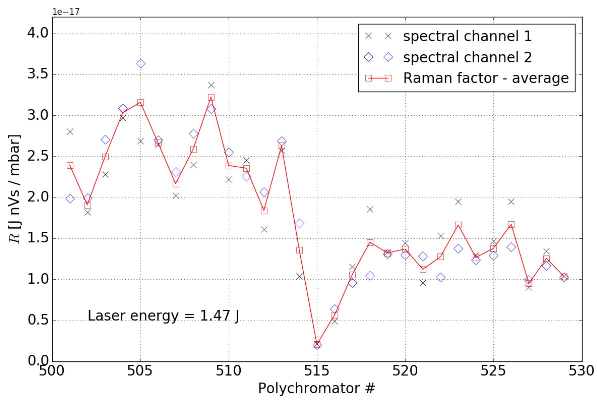

(b)

Fig. 4.12: (a) Integrated Raman signal dependent on gas pressure for the first two spectral channels for polychromator 506. (b) Raman factor computed for all polychromators for laser 1 and pulse 1 (see 4.8). Signal from 1. and 2. spectral channels is averaged.

This method of absolute calibration on the COMPASS tokamak must be performed under strict requirements. First of all, in order not to contaminate cleanness of the tokamak vessel, where high vacuum ($<10^{-5}$Pa) is maintained, a high purity nitrogen (N_2) is used. Gas pressure is limited, due to possible breakdowns in the gas when the value is too high. Experimentally was discovered that the pressure is supposed to be kept under 200 mbar. Additionally, while nitrogen is being filled into vacuum vessel, dust seated on the bottom becomes whirled and possibly is another cause of breakdowns. There is no clear evidence on which is the proper cause, but it is not important issue to be examined. Nevertheless, during Raman calibration gas breakdowns happen randomly and their frequency is increasing with the gas pressure. Light generated this way has different non-Gaussian shape and its intensity might be order of magnitude above saturation limit of detectors. Saturated or otherwise unwanted records must be recognised and removed from the calculation during post processing.

Three methods for bad records recognition are proposed by the author to be implemented to the standard Raman scattering evaluation. First is based on checking saturated records. The sensitivity of each detector and its gain settings state the saturation value for which collected data can be checked. Even saturation of the highest part of the signal peak leads to incorrect determination of fitting parameters. Second routine observes the time evolution of collected light and checks its Gaussian shape. Moreover, due to the character of Raman scattering (see Fig. 4.10) only first two spectral channels of a polychromator are assumed to acquire useful data, therefore detecting signal in third and fourth channel suggests its different nature and these records are excluded. Also records with insufficient intensity of the scattered light, that rarely occur especially when the nitrogen pressure is low, are not used for calculation. Automatic detection of bad records is currently being tested and its optimisation on newly performed Raman scattering measurement is indispensable for its commissioning.

Absolute calibration is resulting in computation of Raman product $R(i)$ for whole set of polychromators, see equation (4.1). Result of most recent calculation for one laser is shown in 4.12b for both first and second spectral channels of each polychromator. The red line signifies the the average value, i.e. the resulting Raman product for each polychromator is taken as an average value. Energy of corresponding laser is given. It can be observed that the Raman product varies significantly with the polychromator number. Polychromators 515 to 529 belong to the edge TS therefore lower values of Raman product are expected, as seen in the figure, mainly due to the linear dependence on scattering length, which defines the spatial resolution of the diagnostics. Edge TS on the COMPASS tokamak has 3 mm resolution, while in the core region it extends to 10 mm, therefore in the edge TS a signal with intensity of approximately one third of core TS is expected. Also more complicated geometry of collection optics of edge TS might decrease the amount of detected signal.

Aim of proposed Raman scattering data processing method is to provide automated system capable of performing self-sufficient calculation of Raman cross section and Raman product for all polychromators, without the necessity of human intervention or supervision, which is nowadays almost inevitable. As mentioned before, achieving this goal still requires series of testing and optimisation process.

By-product of absolute calibration data processing is a creation of configuration file (*config_raman.dat* mentioned in the diagram Fig. 4.9), which contains averaged values of the fitting of temporal evolution of scattered signal, namely pulse peak position $\mathbf{x}_0$ on the time axis[6] and temporal width σ of both the Raman signal and possible stray light, see Fig. 4.8. Meaning of mentioned parameters is given from a form of the Gauss function used during the fitting procedure

[6] $\mathbf{x}$ represents time axis in the ADC unit. This time series is by no means related to tokamak time or triggering system, therefore the $\mathbf{x}$ and $\mathbf{x}_0$ designation. From this point $\mathbf{x}_0$ is called *peak position* and σ*peak width*.

$$\mathbf{f}(\mathbf{x}) = \mathbf{A}\exp\left(-\frac{(\mathbf{x}-\mathbf{x}_0)^2}{2\sigma^2}\right). \tag{4.2}$$

Data from configuration file are planned to be used as initial values for the fitting routine of TS signal during operation, if the parameters show constant tendency. Recent analysis showed the evolution of the parameters $\mathbf{x}_0$ and σ in pursuance of one Raman scattering calibration. Results for polychromator 506 are given in Fig. 4.13, where one can see the evolution of the fitted Gaussian peak parameters, $\mathbf{x}_0$ and σ of the first Gaussian peak (Raman signal). Both figures resemble similar tendency, that with increasing pressure the value of parameters decreases. This feature and its cause is yet to be resolved. Also there is a significant discontinuity between pressure values around 45 mbar, which can be observed in all data sets. This effect is probably caused by changing the ADC gain which is necessary to detect signal of order of magnitude different intensity. In addition, the Fig. 4.13a shows the dependence of $\mathbf{x}_0$ on the laser number. Peak position of laser 1 varies around 616 ns while for the laser 2 around 619 ns. Laser beams are driven to the tokamak vessel by nearly the same laser path, where maximally a 30 cm difference between distances the beams travel could be noticed. The effect is therefore rather caused by a tolerance of electronic components inside laser drivers. On the other hand, the Fig. 4.13b shows the dependency of peak width (σ) on polychromator channel number. The pulse peak width is more related to the characteristics of the detector. Therefore, as each channel is provided with one detector, even though from the same production series, the components characteristics may vary in a range of percent if they fulfil tolerance limit. These phenomena supports the idea to use this values as an initial estimation for given parameters, since it shows that the values are laser or channel specific, although there is a non-negligible trend with respect to nitrogen pressure. Moreover, the parameters of fitted curve show slightly different values across the set of polychromators.

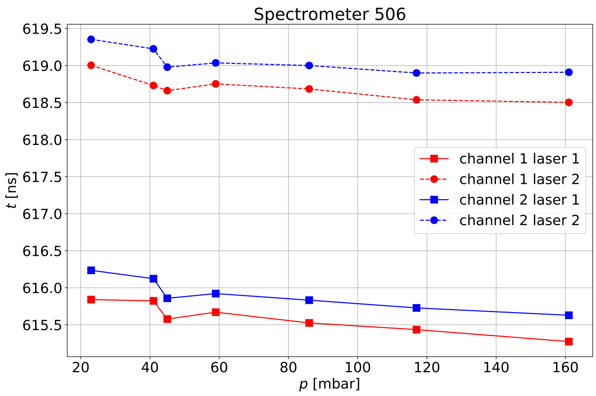

(a)

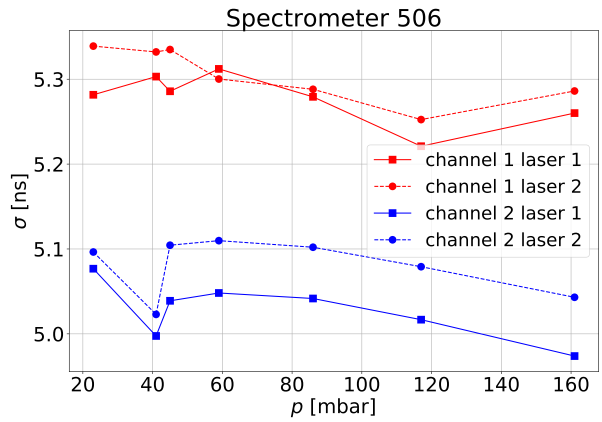

(b)

Fig. 4.13: Results of the fitting routine for latest Raman calibration for first and second channel of polychromator 506 for both lasers: (a) position of the peak center $\mathbf{x}_0$ (b) parameter σ of the gaussian peak.

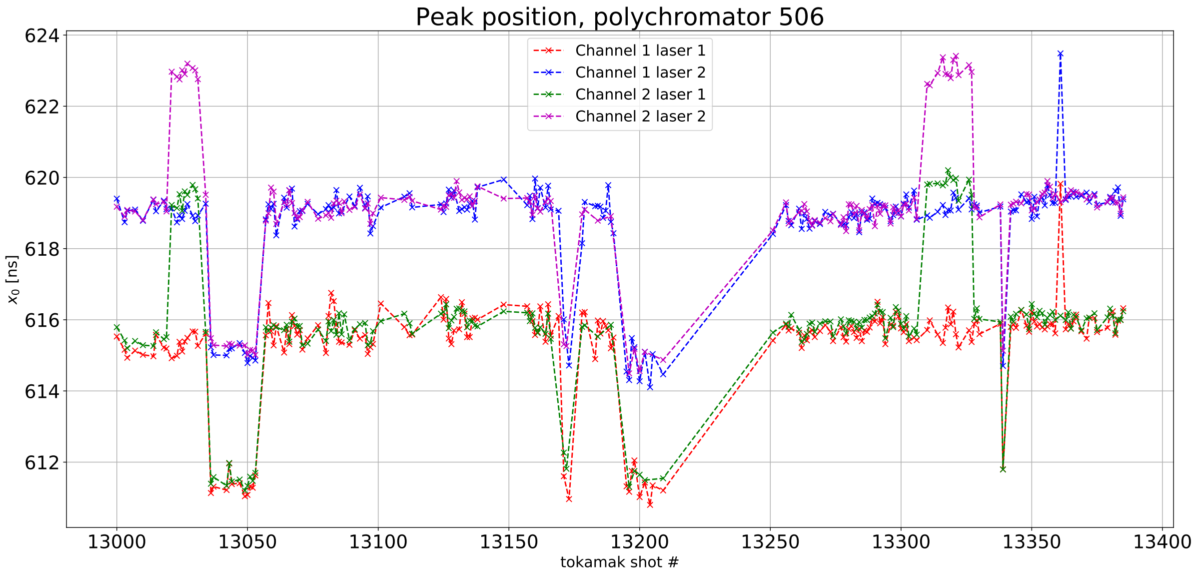

Fig. 4.14: Evolution of the fitting parameter $\mathbf{x}_0$ (signal peak position) for the first two channels of polychromator 506 for both lasers for given tokamak shot range.

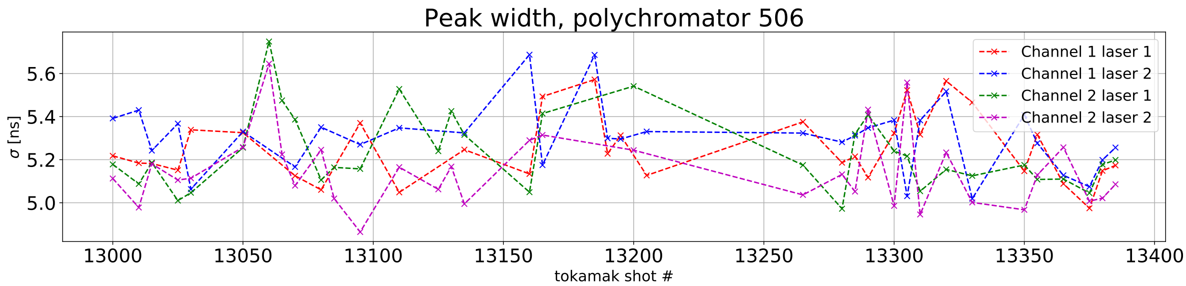

Fig. 4.15: Evolution of the fitting parameter σ (signal peak width) for the first two channels of polychromator 506 for both lasers for given tokamak shot range. Not all successful measurements are displayed, for clarity reasons.

Signal peak position analysis

Alternative approach could take into account all values previously obtained during standard fitting procedure of TS, which is described more in detail in 4.3.3. To perform initial testing a simple routine was written in order to observe the evolution of fitting parameter $\mathbf{x}_0$ for chosen polychromator. Results for the first two channels of the polychromator number 506 in order to provide comparison with previous results on approximately 500 tokamak discharges for both lasers are presented in Fig. 4.14. Firstly, non-constant behaviour of the parameter is apparent. Its value varies from 610 to 625. Significant, from shot to shot, changes of the peak position are observable and would have a negative effect on initial parameter estimation, since the changes are abrupt. Nevertheless if the steps are neglected, slowly increasing trend of the peak position is observed.

If compared with the results presented in the previous section in Fig. 4.13, the values of the main trend (steps excluded) are in a good agreement. For laser 1 for both channels the value fluctuates around 616 ns and for the laser 2 around 619 ns. This outcome indicates possible beneficial usage of this method. Brief analysis shows that some of the steps are result of a change of tokamak and diagnostics operation period, for example day, week or campaign, probably when a complete restart of systems was performed. Additional analysis of the peak position behaviour with emphasis on mentioned sudden changes is necessary in order to prove this method to be useful.

To complete and expand the analysis, a comparison of signal width is useful. Its evolution, described by the parameter σ, for the same period is shown in Fig. 4.15. No similar behaviour of σ to the one shown in Fig. 4.13b is indicated by the displayed data. Values of all channels for both lasers fluctuates between 5.0 to 5.7 with no clear trend. Nevertheless, it seems that it is possible to bound the parameter σ during the fitting routine to a given range and use an average value as initial.

In general, using parameter constriction during the fitting procedure is a very useful and in this case necessary technique in order to perform stable and robust computation. The most important issue is to separate the two peaks, the first containing useful Raman or Thomson scattering data and other one with possible stray light, which is done by bounding the parameter $\mathbf{x}_0$.

Similar computation was performed for the third channel of the polychromator number 507 for approximately 2000 tokamak shots, see Fig. 4.16. Resembling observation can be performed for this case. There could be distinguished several linear trends of the peak position, for instance from tokamak shot number 9100 to 10050 approximately, and then there are several noticeable steps, e.g. after 10050 or 12300. Also various short-time or point deviations from the leading trend occurred, if even consider it as a trend. Gradual degradation or slowly changing properties of electronic components inside control units could cause the drifting features. On the other hand, the issue of synchronisation various hardware clock rates is probably responsible for the sudden steps, since tokamak triggering and data acquisition of TS use their own, and are synchronised every time the systems restart is performed. It could be resolved by using one system clock rate, when it is proven to be the cause.

Furthermore, one can notice the switch between the peak positions of the lasers (blue and red dots) around tokamak shot 11300 and then back again slightly before the shot number 13000. In the concerned area, highlighted by green colour in the figure, input cables for the laser triggering were accidentally swapped with each other. The problem was revealed and fixed afterwards with aid of this routine.

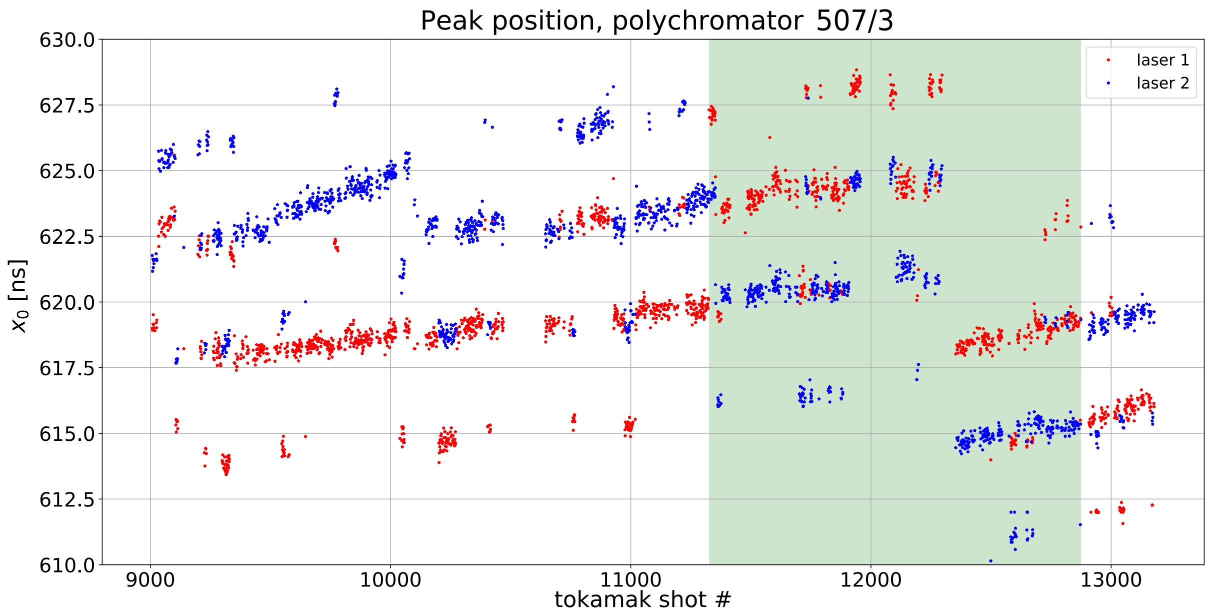

Fig. 4.16: Evolution of the fitting parameter $\mathbf{x}_0$ (signal peak position) for the third channel of polychromator 507 for both lasers with respect to tokamak shot number. Green area represents a period when cables for triggering of lasers were accidentally swapped.

4.3.3 Processing part

Thomson scattering signal processing

As mentioned before in the paragraph **Hardware part**, its outcome consists in two data sets, **TS_data_raw**, where raw data from digitizers are stored, and time series with trigger pulses, which are identified with laser number, from ATCA2 data acquisition device. The goal of the processing routine is to recognize and sort the input data, fit relevant detected signal and integrate the results of calibration in order to provide electron temperature and density.

Firstly, Thomson scattering raw data, demonstrated in Fig. 4.8, are assigned to the right polychromator, channel and spatial point, where the calibration file *spectrometer_mapping.dat* is applied. Standard regime enables 16 measurements by each laser during a tokamak discharge. Only relevant laser shots, when the plasma is present inside the vessel, are chosen to be subsequently processed. Plasma current is a stable measured quantity, that it is used to determine breakdown and duration of discharge, thus the time range for laser shots is stated. Sorted and assigned data are then fitted in time using proper formula, by the same routine as during the absolute calibration process. At this stage, using of initial values for parameter estimation by previously discussed method, is proposed to be integrated. Double Gaussian function $\mathbf{f}_{2G}(\mathbf{x})$, given by 4.3, is proposed as a more suitable function for detected TS and Raman signal on the COMPASS tokamak than single Gaussian, which is used currently. Applying this tool, the influence of stray light is suppressed. Quantities with lower index 1 refer to the TS (Raman) signal, while the stray light is indexed by 2.

$$\mathbf{f}_{2G}(\mathbf{x}) = \underbrace{\mathbf{A}_1 \exp\left(-\frac{(\mathbf{x}-\mathbf{x}_{01})^2}{2\sigma_1^2}\right)}_{\mathbf{f}_1(\mathbf{x})} + \underbrace{\mathbf{A}_2 \exp\left(-\frac{(\mathbf{x}-\mathbf{x}_{02})^2}{2\sigma_2^2}\right)}_{\mathbf{f}_2(\mathbf{x})} \tag{4.3}$$

For illustrative purposes and to clarify meaning of the parameters present in the function, an example of fitting procedure result is shown in 4.17 for one measurement of TS signal. Points (crosses), shown in the figure, represents time evolution of raw data Int_{APD} from APD acquired by digitiser, collected by given polychromator channel, for given laser shots (LS). Two peaks are able to be distinguished, the first one at the position $\mathbf{x}_{01}$ with width σ_1 and much higher intensity $\mathbf{A}_1$ represents TS signal. The second at $\mathbf{x}_{02}$ with σ_2 width and intensity $\mathbf{A}_2$ refers to collected stray light. For illustrations, the graph legend shows fitted values of parameters together with their standard deviation designated by Δ. Due to lower intensity of the stray light signal, noise and uncertainty of the fitting process has more noticeable effect, which results in larger errors. Primarily, when $\mathbf{x}_{02}$ and σ_2 are determined.

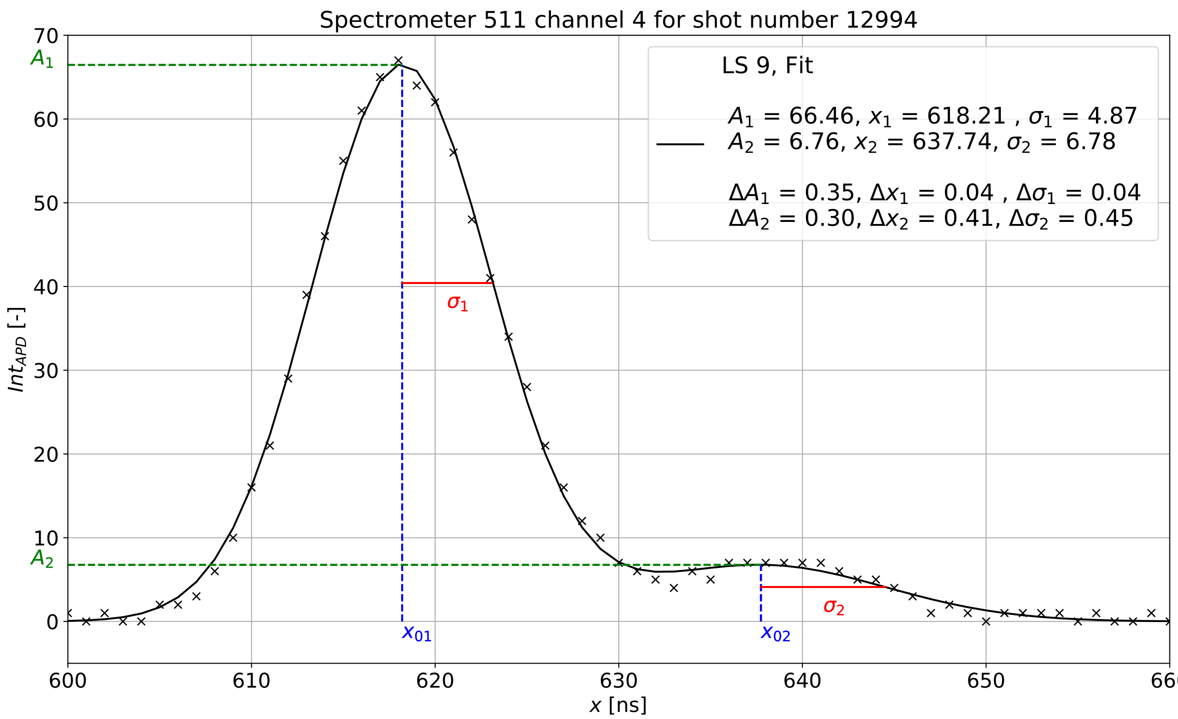

Fig. 4.17: Example result of the fitting procedure using the function 4.3, when applied on detected signal for one Thomson scattering measurement by 4^{th} channel of 511 polychromator with ninth laser pulse during tokamak shot 12994.

Additional examples of results of the fitting procedure of detected signal are shown in the figures Fig. 4.18, to provide more detailed analysis and understanding of this issue. Upper and lower parts of each graph refer to different subsequent laser shots (LS in the legend), where laser number and the laser shot time is specified. As a result of duplexing technique, described in the section 2.2, two regions with measurable signal are supposed to be detected by one polychromator, therefore two main peaks are visible, the first around 620 ns and the second at 680 ns.

Stray light Apart from the TS signal, each of them is followed by another peak of various intensity. It is assumed that the first peak represents useful TS data, while the second one refers to the stray light signal, which is mostly visible from the figure Fig. 4.18a around 640 ns and 720 ns. Such high magnitude of stray light as seen in the same figure of comparable intensity to the first peak of the signal is not a result of a flawless operation and is indicative of a laser misalignment or different mechanical obstruction, that cause undesired reflection or scattering. Standard fitting of shown signal by one Gaussian curve would result in incorrectly estimated parameters.

Proposed method of fitting the signal with double Gaussian curve is able to mitigate or reduce the impact of stray light, as seen from the figure. The dotted line in each graph represents function $\mathbf{f}_1(\mathbf{x})$ from (4.3), therefore only the TS signal. The function corresponds very well with the left half of the peak. As a consequence of the stray light in the right half it deviates to an extent given by the magnitude, width and position of the stray light signal peak. For instance, in 4.18a stray light intensity $\mathbf{A}_2$ is comparable or even larger than TS signal $\mathbf{A}_1$, while in figures (b) and (c) stray light has comparable intensity with the one in (a) but relatively to the TS signal is much lower. It reaches to approximately 15% and 6% of the TS signal in figures (b) and (c), respectively. Black solid and red dashed vertical lines represent boundaries for parameters $\mathbf{x}_{01}$ and $\mathbf{x}_{02}$, respectively. Fitting range is given specifically for each polychromator, channel and laser number, which was at this stage based on the observation of parameters of standard TS data. Difference between the two laser pulses was discussed previously and the relative shift of approximately 4 ns is considered. Design of detectors, shown in 2.1 and one polychromator more in detail in 2.3a, gives different time of flight of collected light towards one channel and APD. The distance the light travels between two filters is approximately 30 cm, therefore in takes 1 ns. As seen from figures (b) and (c), for LS 9 the first peak on the third channel $\mathbf{x}_{01}$ = 616.21 ns while for the same LS the fourth channel gives $\mathbf{x}_{01}$ = 619.24, therefore the difference is three times higher. It suggests that other factors than the time of flight have substantial impact.

Examination of the stray light peak position could help with determination of its origin and possible source. From Fig. 4.18a one can notice that the stray light is delayed by $\Delta t_{SL} \approx$ (643 - 623) ns = 20 ns. Over this time light travel the distance of approximately 6 meters. As mentioned in the section 2.1 about laser system on the COMPASS tokamak, laser beam path is terminated by a beam dump situated 2.5 meters below the horizontal axis of vacuum vessel. When both the distance towards the beam dump and back to the plasma region are considered, it correspond well with the stray light delay. Probably an unwanted reflection or dispersion of the laser light happens on the laser beam dump or when it travels through laser path. To illustrate the effect of undesirable reflection, in the Fig. 4.19 is shown the signal from one tokamak discharge, when one of the shutters in the laser beam path beneath the tokamak vessel was not

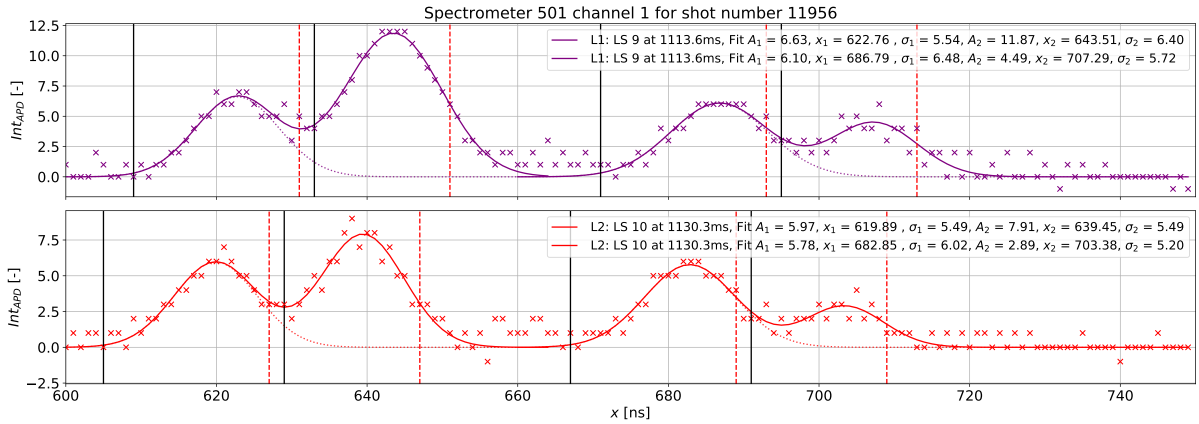

(a)

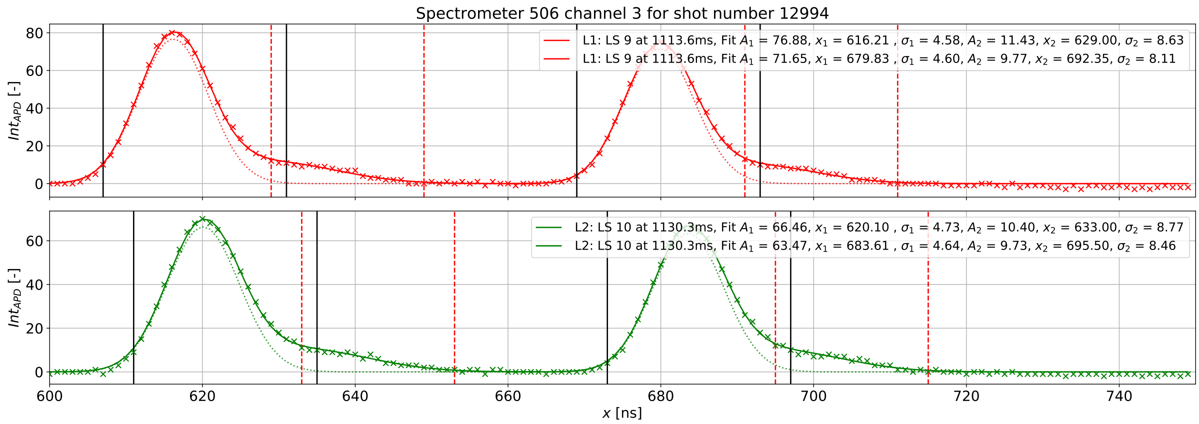

(b)

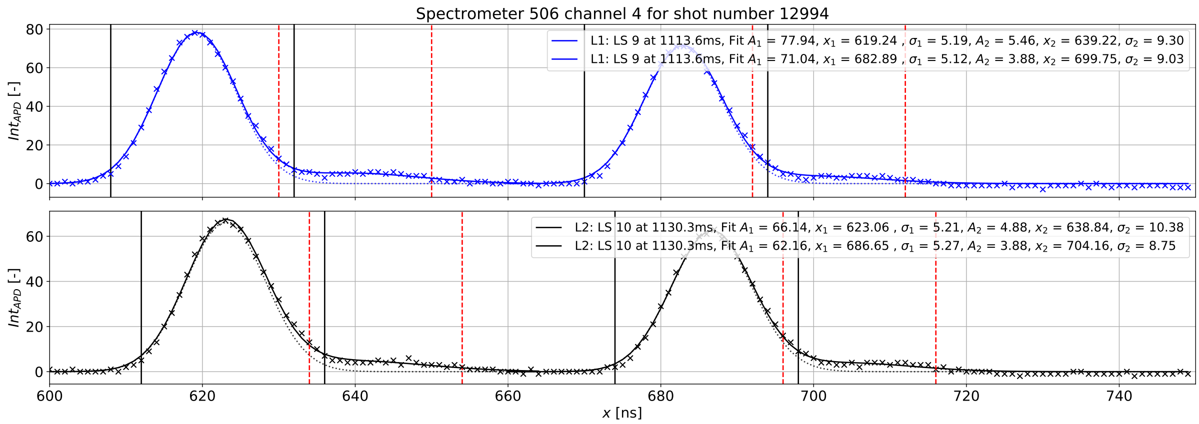

(c)

Fig. 4.18: Example of the fitting procedure of TS signal for polychromator (a) 501, channel 1 (b) 506, channel 3 (c) 506, channel 4. Both peaks, which are result of the duplexing method, are processed. Fitted parameters match their description in 4.3. Dotted line represents Gaussian shaped curve of TS signal only, i.e. $\mathbf{f}_1(\mathbf{x})$.

open properly and partly cut off one of the laser beams, thus becoming a significant source of stray light. The figure shows detected signal from 2 laser shots of each laser by first and second channel of the of polychromator 505. Significant stray light is most observable in upper part of Fig. 4.19a and also to some extent in Fig. 4.19b, therefore only for laser 1 (L1), which is probably caused by a difference between beam path of the lasers. Clearly, the stray signal is laser induced, because in each laser shot it arrives at the same moment after the useful signal. Third and fourth channels are not shown, as the stray light signal is not so noticeable, but neither negligible. The fact that the highest intensity signal is acquired by the first channel, suggest that the wavelength of signal is rather close to the wavelength range of the first spectral filter. When the obstruction was removed stray light of this intensity disappeared.

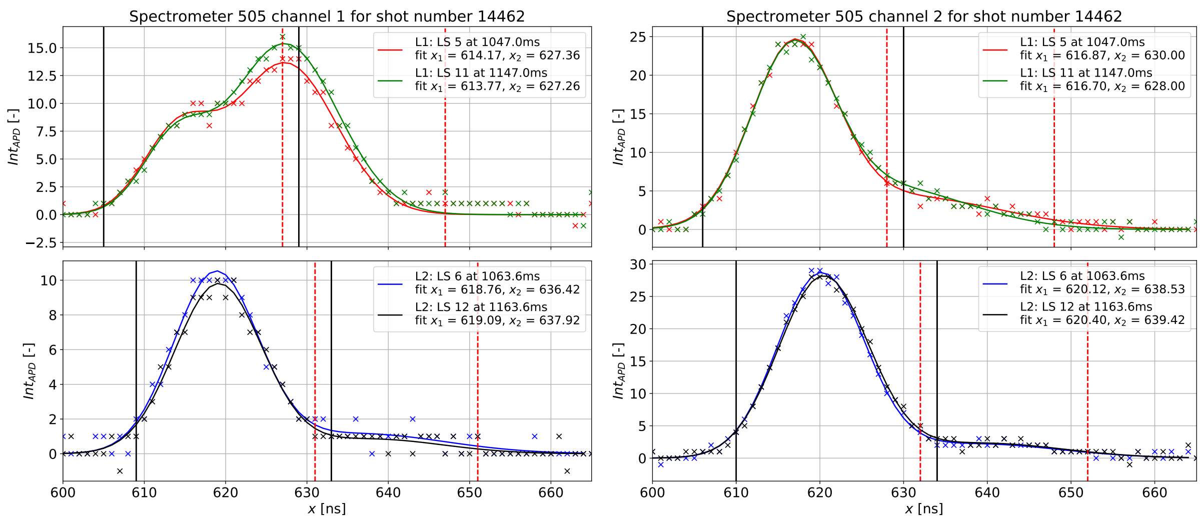

(a) (b)

Fig. 4.19: TS data detected by (a) 1. and (b) second channel of polychromator 505 for two laser shots (LS) of each laser (L1,L2) at different times during the plasma discharge. Parameters of the fitting function are not shown to achieve figure clarity.

Considering figures 4.18b and 4.18c, if shown fitted curves are examined in the same way, estimated relative delay Δt_{SL} of what is assumed to be a stray light peak is different, namely varies around 13 ns for 3rd channel of spectrometer 506 and from 16 to 20 for its 4th channel. Firstly, this effect could be a result of the fitting routine, due to lower intensity of stray light and the fact that it could not be distinguished from the TS signal. Both peaks merges together and more than two Gaussian peaks it resembles an asymmetrical Gaussian with elongated right tail. Even though the double Gaussian function fits the data very well with small deviation, it is not certain that the detected signal is the combination of two Gaussian functions. Further analysis and searching proper function could result in more accurate fitting and thus the whole diagnostic system.

Moreover, the issue of asymmetrical Gaussian function could be related to the fact, that response of an APD is not linear and during a decline of signal the voltage decreases more slowly. Larger right tail of detected peak could be caused by this effect, which is yet not implemented to the fitting routine. Examination of laser pulse temporal evolution profile also aids to clarify the shape of detected signal. As a confirmation of such phenomenon, it is useful to measure small portion of laser pulse itself before it enters the tokamak vessel and check if its profile corresponds or resembles afterwards detected signal. Performing this method certainly improves the overall diagnostics reliability and is currently being discussed to be implemented. Possible secondary peaks or non-Gaussian temporal profile of the laser pulse could be detected. To support the fact, that TS signal is asymmetric due to imperfection of laser pulse, it was discovered that the deviation is strictly associated to the detection of the first peak. Once the plasma is terminated, several laser pulses are fired through the tokamak vessel, where none stray light signal is observed. This confirms the statement that the stray light is originated when laser pulse interacts with plasma.

On the other hand, this effect also supports the idea that it is caused by stray light, but, rather than unwanted reflection from the beam dump or path, randomly reflected light of the useful signal to the collection optics from inner components of tokamak vessel. Moreover, as seen from 4.19, unambiguous stray light cause by laser misalignment is recorded mostly by first spectral channel. Since this effect is applied for all channels, it suggests similar wavelength range of stray light as the useful signal to be able to reach third and fourth channel.

At this stage, there is no significant evidence for either of proposed hypotheses and further examination and implementation of suggested method to observe output laser pulse temporal evolution is necessary.

Electron temperature and density determination

Assuming the TS signal Int_{TS} in each channel has already been detected, separated and fitted, afterwards integrated in time must be performed. It could be calculated analytically from the fitting curve parameters using a formula:

$$I_n = \int_{t_{min}}^{t_{max}} Int_{TS}(n)\ \mathrm{d}t \cong \int_0^{\infty} \mathbf{f}_{1_n}(\mathbf{x})\mathrm{d}\mathbf{x} = \int_0^{\infty} \mathbf{A}_1 \exp\left(-\frac{(\mathbf{x}-\mathbf{x}_{01})^2}{2\sigma_1^2}\right)\mathrm{d}\mathbf{x} = \sqrt{2\pi}\sigma_1\mathbf{A}_1 \tag{4.4}$$

using standard Gaussian integral for n-th channel, where the meaning of variables is explained by (4.3). Bounds for integration t_{min} and t_{max} simply indicates that only useful data restricted by this range are included during calculation. From time integrated TS signal for each polychromator channel, one can easily obtain *Ratios of signal in channels* and *Intensity in channels*. From these quantities, which are included in the diagram Fig. 4.9, electron temperature and density are calculated when combined with calibration results. Based on the theoretical background, the Doppler shifted spectrum of Thomson scattering signal for different temperatures can be determined, see Fig. 1.3. Performing spectral calibration process, when spectral transmittance of polychromator channels (Fig. 2.3b) is measured, enables estimation of ratios of intensities in two following channels (**2 : 1**, **3 : 2**, **4 : 3**) as a function of electron temperature, shown in Fig. 4.20. Final data are used when measured ratios are fitted to correspond them. Total intensity in all channels is proportional to electron density when the results from absolute calibration and laser energy measurements are used. Both calculations are performed simultaneously during one fitting procedure, but are separated in the diagram to maintain simplicity.

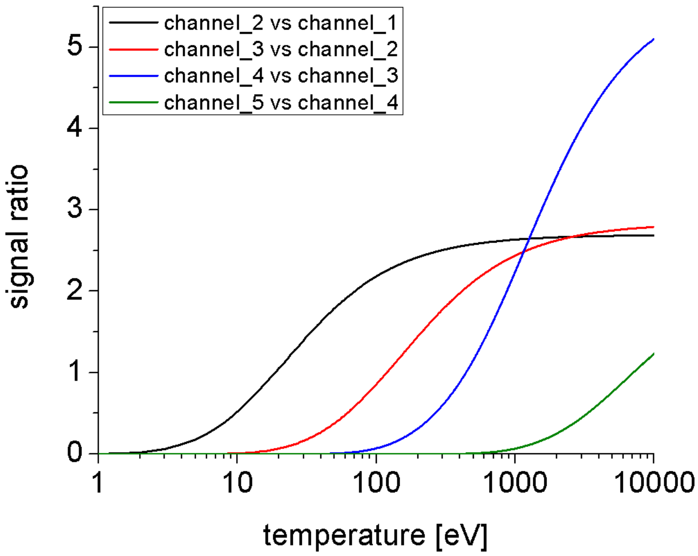

Fig. 4.20: Ratios of channel signals as a function of electron temperature [11].

Last stage of the data processing algorithm consists in assigning calculated values to the right time and position. Results from spatial calibration are used to assign measured data to tokamak **z-axis** position. For temporal assignment laser shot trigger time marks from ATCA2 are used. Overall result of the data processing unit of TS diagnostics on the COMPASS tokamak consists in data sets containing profile of electron temperature T_e and density n_e as a function of vertical position along the laser beam axis (**z_axis**) for each relevant laser shot during the plasma discharge. Under certain conditions, profile of plasma pressure p_e can be determined as a product of temperature and density. To determine error of plasma pressure, the covariance matrix from T_e, n_e fitting is necessary.

Summary

Thomson scattering diagnostics on the COMPASS tokamak is currently being expanded into four laser system and reliable technique for alignment would substantially assist with its control and maintenance. In addition, collection optics underwent also major enhancement, when the objective and optical fibre holder were replaced for more suitable to exploit recently modified viewing port for the edge TS. Results are yet to be published [Bohm LAPD 2017]

Laser beam alignment

As mentioned in the section 4.1, proper camera for the laser beam alignment was evaluated and purchased. Initial tests were performed with purchased camera as seen in Fig. 4.6. Moreover, several other applications for the camera were found, for instance during the spatial calibration, images of the back-illuminated fibre bundles by an infra-red diode were observed or as a viewing tool during the laser path alignment when hardly accessible position was necessary to be observed.

In the beginning of the year 2017 an updated version of SDK was released where, in addition to other upgrades, Python should be supported. The plan is to develop and implement the algorithm, which is proposed in Fig. 4.7, in Python programming language.

Due to mentioned upgrade in TS diagnostics and new SDK release supporting Python, the authors effort was concentrated more on the data processing part. Once the upgrade is finished, the work on the automated laser beam alignment using camera and motorised windows will be restored. The usage of new SDK will be investigated in order to implement the system as a part of the diploma thesis.

Thomson scattering data processing part

Thomson scattering data processing is currently performed by a set of routines in IDL programming language, which are not perfectly robust, stable and does not provide variability. Proposed idea to translate them to Python could help or even solve some of mentioned problems, especially concerning temporal fitting of raw signal or calibration process.

At this moment, a set of routines providing data processing of Thomson scattering diagnostics in Python is under development and is being prepared for commissioning, while only the last part shown in Fig. 4.21 of the main algorithm Fig. 4.9 is missing. It is expected to be implemented in the next few months.

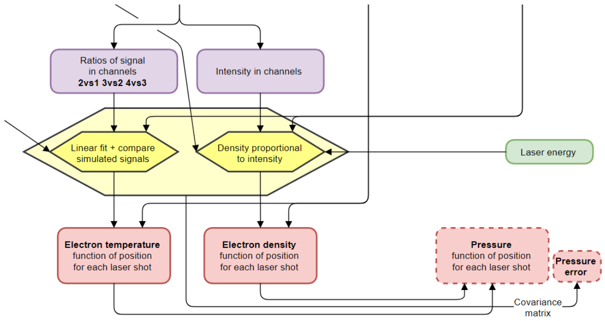

Fig. 4.21: Final segment of the data processing algorithm Fig. 4.9, which was not yet implemented by the author in Python environment.

There is a strong emphasis on the robustness, stability and to some extent variability of the whole calculation sequence in order to provide reliable data processing unit. Moreover, calibration process is planned to be calculated and evaluated automatically, without the necessity of supervision from the personnel side, but with the possibility to intervene and remove incorrect data.

Concerning the main TS calculation, the importance and benefits of proposed improvements especially regarding temporal fitting of TS signal and stray light mitigation are discussed above. The tendency is to provide self-sufficient set of routines in Python programming language capable of performing calculations of both calibration processes and standard TS diagnostics operation. The aim is to create as robust, optimised and stable processing unit as possible, providing certain level of variability, especially for the fitting part, and visualisation of some intermediate and final results, that can become a standard tool for TS diagnostic data processing tasks.

Bibliography

[1] B. Kurzan, et al. Signal processing of Thomson scattering data in a noisy environment in ASDEX upgrade. *Plasma Phys. Control. Fusion*, 46:299–317, 2004.

[2] FLIR Knowledge Base. How to evaluate camera sensitivity. `https://eu.ptgrey.com/KB/10912`. [Online; accessed 14/3/2017].

[3] FLIR Knowledge Base. Selecting a lens for your camera. `https://eu.ptgrey.com/KB/10694`. [Online; accessed 15/3/2017].

[4] P. Böhm. *Temporally and spatially resolved evolution of plasma in the COMPASS tokamak*. PhD thesis, Czech Technical University in Prague, Faculty of Nuclear Sciences and Physical Engineering, 2011.

[5] N.C. Luhmann Jr. D.H. Froula, S.H. Glenzer and J. Sheffield. *Plasma Scattering of Electromagnetic Radiation: Theory and Measurement Techniques*. Academic Press; 2 edition, nov 2010. DOI: 10.1016/C2009-0-20048-1, ISBN: 978-0123748775.

[6] EUROfusion. JET's main features. `https://www.euro-fusion.org/jet/jets-main-features/`. [Online; accessed 12/1/2017].

[7] ITER Organization. ITER - the way to new energy. `https://www.iter.org/`. [Online; accessed 12/1/2017].

[8] J. Sheffield, et al. Plasma Scattering of Electromagnetic Radiation. *Academic Press*, 2011. Burlington, USA, ISBN 978-0-12-374877-5.

[9] P. Kulhánek. *Úvod do teorie plazmatu*. AGA (Aldebaran Group for Astrophysics), 2011. ISBN 978-80-904582-2-2.

[10] J. D. Lawson. *Some criteria for a Power producing thermonuclear reactor (Technical report)*. Atomic Energy Research Establishment, 1955. Harwell, Berkshire, U.K.

[11] M. Aftanas, et al. Thomson scattering on COMPASS - commissioning and first data. *JINST*, 7(C01074), 2012.

[12] Max-Planck-Gesellschaft. Introduction: the ASDEX Upgrade tokamak. `http://www.ipp.mpg.de/16208/einfuehrung`. [Online; accessed 12/1/2017].

[13] K. Miyamoto. *Plasma Physics and Controlled Nuclear Fusion*, volume 38 of *Springer Series on Atomic, Optical, and Plasma Physics*. Springer-Verlag Berlin Heidelberg, 2005. doi: 10.1007/3-540-28097-9.

[14] Institute of Plasma Physics of the CAS. COMPASS tokamak. `http://www.ipp.cas.cz/vedecka_struktura_ufp/tokamak/tokamak_compass/`. [Online; accessed 12/1/2017].

[15] P. Böhm, et al. Edge Thomson scattering diagnostic on COMPASS tokamak: Installation, calibration, operation, improvements. *Rev. Sci. Instrum.*, 85(11E431), 2014.

[16] P. Böhm, et al. Fitting of the Thomson scattering density and temperature profiles on the COMPASS tokamak. *Rev. Sci. Instrum.*, 87(11E536), 2016.

[17] P. Bílková, et al. Design of Thomson scattering diagnostic system on COMPASS tokamak. *Nucl. Instrum. and Meth. in Phys. Res. A*, pages 1273–1276, 2010.

[18] P. Bílková, et al. Progress of development of Thomson scattering diagnostic system on COMPASS. *Rev. Sci. Instrum.*, 81(10D531), 2010.

[19] C. M. Penney, R. L. St. Peters, and M. Lapp. Absolute rotational raman cross sections for n2, o2, and co2. *J. Opt. Soc. Am.*, 64(5):712–716, May 1974.

[20] S. L. Prunty. A primer on the theory of Thomson scattering for high-temperature fusion plasmas. *Phys. Scr.*, 89, 2014.

[21] R. Scannell, et al. Design of a new Nd:YAG Thomson scattering system fot MAST. *Rev. Sci. Instrum.*, 79(10E730), 2008.

[22] R. Scannell, et al. A 130 point Nd:YAG Thomson scattering diagnostic on MAST. *Rev. Sci. Instrum.*, 81(10D520), 2010.

[23] R. Scannel. *Investigation of H-mode edge profile behaviour on MAST using Thomson scattering*. PhD thesis, 2007.

[24] M. Sos. *Tokamak plasma diagnostic based on Thomson scattering - calibration*. Bachelor thesis, Czech Technical University in Prague, Faculty of Nuclear Sciences and Physical Engineering, 2015.

[25] J. Wesson. *Tokamaks*. Oxford Engineering Science Series. Oxford University Press; 2 edition, 1997. ISBN: 9780199592234.

List of Figures

List of Tables